Accepted manuscript:

Vanadium and its isotope composition of river water and seawater: Analytical improvement and implications for vanadium isotope fractionation

by
Stephan Schuth 1*, Annika Brüske 1, Simon V. Hohl 2,3, Shao-Yong Jiang 2,4 , Ann-Katrin Meinhardt 5, Daniel D. Gregory 6, Sebastian Viehmann 7, and Stefan Weyer 1

1 Institute for Mineralogy, Leibniz University Hannover, 30167 Hannover, Germany
2 Department of Earth Sciences, Nanjing University, 210093 Nanjing, P.R. China
3 School of Ocean and Earth Science, Tongji University, 2000092 Shanghai, P.R. China
4 State Key Laboratory of Geological Processes and Mineral Resources, Faculty of Earth Resources, China University of Geosciences, 430074 Wuhan, P.R. China
5 Institute for Chemistry and Biology of the Marine Environment, Carl von Ossietzky University Oldenburg, 26111 Oldenburg, Germany
6 Department of Earth Sciences, University of Toronto, M5S 3B1 Toronto, Canada
7 Department of Geodynamics and Sedimentology, University Vienna, 1090 Wien, Austria

https://doi.org/10.1016/j.chemgeo.2019.07.036

Received 24 April 2019; Received in revised form 13 July 2019; Accepted 30 July 2019
Available online 10 August 2019 (Embargo: 24 months)

Vanadium and its isotope composition of river water and seawater: analytical improvement and implications for vanadium isotope fractionation

Stephan Schuth [1*], Annika Brüske [1], Simon V. Hohl [2,3], Shao-Yong Jiang [2,4], Ann-Katrin Meinhardt [5], Daniel D. Gregory [6], Sebastian Viehmann [7], and Stefan Weyer [1]

[1] Institute for Mineralogy, Leibniz University Hannover, 30167 Hannover, Germany
[2] Department of Earth Sciences, Nanjing University, 210093 Nanjing, P.R. China
[3] School of Ocean and Earth Science, Tongji University, 2000092 Shanghai, P.R. China
[4] State Key Laboratory of Geological Processes and Mineral Resources, Faculty of Earth Resources, China University of Geosciences, 430074 Wuhan, P.R. China
[5] Institute for Chemistry and Biology of the Marine Environment, Carl von Ossietzky University Oldenburg, 26111 Oldenburg, Germany
[6] Department of Earth Sciences, University of Toronto, M5S 3B1 Toronto, Canada
[7] Department of Geodynamics and Sedimentology, University Vienna, 1090 Wien, Austria

[*] Corresponding author, e-mail: s.schuth@mineralogie.uni-hannover.de

Keywords: Vanadium, isotopes, seawater, river water, Yangtze River Basin

Highlights:

- First vanadium isotope signatures reveal a large spread of up to ca. 2 ‰ between dissolved and particulate-bound V of rivers in the Yangtze River Basin
- V isotope fractionation in rivers is affected by V adsorption to particulate Fe oxides
- Improved method of V separation from seawater allows for handling of large sample volumes at >90 % V recovery for UV-irradiated solutions
- V isotope signatures of coastal North Sea water are slightly lower when compared to the major oceans and may indicate a mixture of river and seawater

Abstract

Investigation of redox variations in recent and paleo-oceans has been of particular scientific interest to elucidate the rise and variations of the atmospheric oxygen level by analyses of isotopic signatures of redox-sensitive elements like Fe, Mo, and U. Vanadium is another redox-sensitive metal that has become the target of stable isotope research during the last decade. The oceanic V cycle can be simplified to consist of one major source represented by rivers and two major sinks (sediments, hydrothermal activity at mid-ocean ridges). The balance between these major V pools is sensitive to the ocean water oxygen level and chemistry. However, the data set of stable V isotope signatures of seawater is still very small, and the riverine V isotope composition, i.e. the major source of V in modern marine environments, has not been constrained at all so far.

In this study, we present a new method for efficient V separation from seawater that allows multiple analyses of the V isotope composition of a single sample. To separate V from large amounts (volume ≥ 2 L) of seawater samples, we employ the Bio-Rad® Chelex-100 resin and conventional cation and anion resins to yield a high V recovery of ≥90 % from an UV-irradiated sample. Non-irradiated samples were marked by lower V recovery rates of ca. 75 %, which was also observed in earlier studies. Further tests however revealed that even such reduced V yields do not incur significant V isotope fractionation within analytical uncertainty. Our $\delta^{51}V_{AA}$ value of +0.30 ‰ ±0.14 (2s.d., n=3) for the NASS-6 seawater reference solution perfectly matched earlier results. In addition, seawater collected in the Wadden Sea at the German North Sea coast is marked by a $\delta^{51}V_{AA}$ signature of +0.03 ‰ ±0.19 (2s.d., n=17), which is slightly lower than those of the great oceans, and may be related to an influx of river water, bioactivity, or a tide-induced V mobilization.

To characterize the V isotope composition of the major V source to the oceans, we determined for the first time V isotope signatures of 13 selected rivers (dissolved and particulate fractions of source water, tributary rivers, and the Yangtze River) in the Yangtze River Basin, China. A large variation of dissolved V (ca. 0.07 to 6.0 µg/L) and particulate-bound V (ca. 0.03 to 17 µg/L) was found for the sample suite. The obtained $\delta^{51}V_{AA}$ values of the dissolved V pool span a range of -0.79 ‰ (±0.18; 2s.d.) to -0.13 ‰ (±0.22, 2s.d.), whereas particulate-bound V extends to lower $\delta^{51}V$ signatures between -2.16 ‰ (±0.30, 2s.d.) and -0.14 ‰ (±0.11, 2s.d.). Notably, dissolved V from the river sources and small tributaries scatters between ca. -0.45 ‰ to -0.75 ‰, and agrees well with the predicted average $\delta^{51}V_{AA}$ value of -0.6 ‰ ±0.3 for continental run-off by Wu et al. (2019). For the lower

Yangtze River, however, the dissolved $\delta^{51}V_{AA}$ signatures increase from the Three-Gorges Dam towards the estuary from -0.79 ‰ to -0.13 ‰, suggesting V isotope fractionation due to adsorption to abundant particulate Fe oxides, but may also reflect an input of anthropogenic V. The low $\delta^{51}V_{AA}$ of particulate V largely follow this trend, and thus indicate ongoing V isotope fractionation during riverine V transport to the ocean.

Our first results of stable V isotope investigation of river waters show that V isotope signatures can indeed carry their host rock signature, but are also sensitive to adsorption-driven fractionation in oxidized environments. The latter strongly depends, as predicted from earlier theoretical calculations, on the presence of particulate Fe-(oxyhydr)oxides and highlights gradual V isotope fractionation during riverine V transport to the ocean.

1 Introduction

The stable isotope signatures of several transition and heavy metals are now intensively used in (bio-)geochemistry studies, highlighting their potential to investigate biotic and abiotic processes over a large temperature range from low-temperature surface water systems (e.g., seawater, rivers) to high-temperature (e.g., magmatic, hydrothermal) environments. Redox sensitive metals and their isotopic signature have been widely used to reconstruct the rise of atmosphere oxygen or the oxygenation and redox fluctuations of oceans throughout Earth's history (e.g., Algeo et al., 2011; Catling and Claire, 2005; Lyons et al., 2014, Gregory et al., 2017), and periodic anoxic ocean events during the Phanerozoic (e.g., Erbacher et al., 2001; Tribovillard et al., 2006; Brennecka et al., 2011; Large et al., 2015). Stable isotope analyses of redox-sensitive elements like S, Cr, Fe, Mo, and U have shown that changes in their valence state due to variations of oceanic redox conditions can result in significant isotope fractionation. The combined investigation of different stable isotope systems during the last decade has significantly improved the understanding of global paleo-ocean redox variations, the evolution of atmospheric and hydrospheric oxygen levels, and the emergence of early life (e.g., Anbar, 2004; Bjerrum and Canfield, 2004; Johnson et al., 2008; Shen et al., 2001; Montoya-Pino et al., 2010; Lau et al., 2017). Most isotopic redox proxies used in earlier studies have only two stable valence states occurring in marine settings, e.g., $U^{(IV)}$-$U^{(VI)}$, $Mo^{(IV)}$-$Mo^{(VI)}$, and $Fe^{(II)}$-$Fe^{(III)}$. Hence, isotope fractionation related to redox changes in a given setting is probably sensitive only to a small window in E_h

vs. isotope space. Alternatively, redox-sensitive poly-isotopic elements having more than two valence states in different natural settings may serve for detailed investigation of marine redox changes over a large range on a local and global scale. Vanadium is such a promising candidate, for which typically three valence states are stable (e.g., Takeno, 2005), and which occurs in a similar or higher abundance in many sediments and ocean water when compared to Fe, Mo, and U (e.g., Nriagu, 1998; Sohrin and Bruland, 2011).

In this study, we want to address for the first time the V isotope systematics of rivers, the major V input to oceans at present. To shed even more light on the riverine V isotope signature, we investigated the V isotope composition of both the dissolved and the particulate V load in river water samples. However, because the dissolved V concentration in rivers is typically low (<0.8 µg/L, e.g., Huang et al., 2015; Schlesinger et al., 2017; Gustafsson, 2019), several analytical challenges need to be resolved for a successful V isotope determination in such low-V matrices. As a target area for a case study and method development for V isotope analyses in river samples, we sampled the Yangtze River, located in south-east China, at different locations and several of its tributaries. In addition, a water sample from the Wadden Sea (German North Sea coast) was analyzed to extend the currently small V isotope data set of seawater (Wu et al., 2019). We will show that (i) our methods are straightforward in use and capable of providing accurate results in a timely manner, and (ii) analyses of reference materials are in excellent agreement with those of Wu et al. (2019).

2 Systematics of vanadium and its isotopes

2.1 Vanadium geochemistry

In low-temperature oxidized environments like oceans and rivers, vanadium is most common in the pentavalent (V^{V}) and the tetravalent (V^{IV}) oxidation states (see reviews by e.g., Nriagu, 1998; Huang et al., 2015; Gustafsson, 2019). The occurrence of trivalent V (V^{III}) is largely restricted to euxinic environments (e.g., Breit and Wanty, 1991; Wanty and Goldhaber, 1992; Gustafsson, 2019). Divalent V (V^{II}) V^{III} and V^{II} could play a role as a redox couple in biologic processes (e.g., Zhang et al., 2014; Van Marwijk et al., 2009; Ueki et al., 2003; Bredberg et al., 2004). In addition, V^{II} can be used in one half-cell of vanadium redox-

flow batteries (e.g., Li et al., 2011). The speciation of V in aqueous solutions depends on parameters like E_h, pH, V concentration, and the amount of dissolved complexing agents, such as organic ligands, sulfur compounds, and hydrolyzed complexes (e.g., Huang et al., 2015; Emerson and Huested, 1991; Zhou et al., 2011; Gustafsson, 2019). In oxygenated water with near neutral pH like in modern rivers, V is typically present in the form of various soluble pentavalent vanadate complexes, e.g., $HV^{V}O_4^{2-}$, and $H_2V^{V}O_4^{-}$ (e.g., Sohrin and Bruland, 2011; Chester, 2000; Gustafsson, 2019). In modern oceans, V remains largely complexed as vanadate oxyanions and, therefore, has a rather long residence time of roughly 50 to 80 ka (e.g., Schlesinger et al., 2017; Tribovillard et al., 2006; Chester, 2000). The concentration of V in modern ocean water is on average typically lower than 2 µg/L (e.g., Jeandel et al., 1987; Sohrin and Bruland, 2011; Emerson and Huested, 1991; Huang et al., 2015). Under reducing conditions and depending on pH, the presence of tetravalent vanadyl ions ($V^{IV}O^{2+}$, pH <6) and V-oxyhydroxyl ions ($V^{III}OH^{2+}$, pH <5) increases, which can be further reduced and transformed into poorly soluble V-hydroxides like $V^{III}(OH)_3$ at strongly reducing conditions (e.g., Breit and Wanty, 1991; Allison et al., 1994; Gustafsson, 2019). Consequently, at oceanic pH of around 8 the concentration of dissolved V decreases dramatically at low E_h (e.g., Tribovillard et al., 2006; Emerson and Huested, 1991; Shiller and Mao, 1999; Wehrli and Stumm, 1989). The geochemistry of V is furthermore strongly influenced by its sorption potential to minerals, colloids, and organic matter. For example, dissolved V can be efficiently adsorbed onto particle surfaces and also scavenged during precipitation of e.g. Mn- and Fe-(oxyhydr)oxides (e.g., Brinza et al., 2008; Brumsack, 2006; Gustafsson, 2019; Prathap and Namasivayam, 2010; Schwertmann and Pfab, 1994; Trefry and Metz, 1989). The fixation of V by Fe-(oxyhydr)oxides is particularly interesting at present-day oceanic pH in oxygenated water, where such Fe-(oxyhydr) oxides precipitate rapidly e.g. at hydrothermal vents or form during alteration of the oceanic crust. Geochemical models have concluded that the overall oceanic V budget is partly controlled by V scavenging in hydrothermal systems and sedimentation respective Fe-Mn nodule formation (Morford and Emerson, 1999; Trefry and Metz, 1989; German et al., 1991; Gustafsson, 2019). As present-day oceans and rivers are largely oxygenated, the V removal in anoxic or euxinic water bodies constitutes only a minor process (e.g., Schlesinger et al., 2017). The latter, however, still played an important role for local and/or temporary processes throughout Earth history when pO_2 levels were lower than today. For example, V

enrichment of up to several 1,000's of µg/g is reported from organic carbon-rich Phanerozoic black shales that deposited under strongly reducing conditions (e.g., Xu et al., 2012, 2013). In this case, V can be incorporated into porphyrins (Lewan and Maynard, 1982; Parnell et al., 2001; Tribovillard et al., 2006), adsorbed to clay minerals, or alternatively be immobilized as V_2O_3 or $V(OH)_3$ (e.g., Breit and Wanty, 1991). In contrast to modern well oxygenated oceans, most marine sediments of early Earth's history were deposited in largely anoxic to euxinic environments and, thus, may have been a dominant V sink, as assumed for other redox-sensitive metals like Mo and U (e.g., Weyer et al., 2008; Tribovillard et al., 2006; Anbar, 2004; Emerson and Huested, 1991; Algeo and Maynard, 2004; Kendall et al., 2013; Rouxel et al., 2005).

The oceanic V cycle can be simplified to consist of one major source and two major sinks, as illustrated in Fig. 1. Rivers constitute the most significant V input because of high V mobility in oxygenated water and during oxidative weathering (e.g., Das and Krishnaswami, 2007; Shiller and Mao, 2000), although the V concentration of the granitic upper continental crust is low relative to that of MORB (e.g., Nriagu, 1998). Furthermore, fluctuating redox conditions from reducing to oxidizing conditions, e.g. due to seasonal variations, within 1 cm of a sediment layer at a continental margin have been discussed to contribute a similar V flux to the ocean water as riverine input (Morford and Emerson, 1999). Sources such as volcanic activity and sinks such as euxinic sediments play only a minor role for the modern V cycle in seawater (e.g., Schlesinger et al., 2017). As major sinks of V in the modern V marine cycle, carbonate platforms, shelf and deep sea sediments (e.g. red clays), Fe-Mn nodules, and to a lesser degree also hydrothermal activity, have been put forward (e.g., Schlesinger et al., 2017; Morford and Emerson, 1999). The balance between the major V pools is very sensitive to fluctuations of ocean water oxygenation and chemistry. For example, according to model calculations, changes in seawater level resulted in a decrease of ocean water vanadium by 6 to 14 % during the last 20 ka because the area of shelf sediments that are subject to more reducing conditions (and therefore acting as V sinks) increased due to a rise of the seawater level at the end of the last glaciation (Morford and Emerson, 1999). A potential enrichment of V by a higher river runoff is discussed e.g. for V/Ca in corals in the South China Sea during the 20th century because of an increasing anthropogenic input of trace metals like V that are mobile in oxidizing environments (Chen et al., 2015). For aquatic organisms like certain algae and daphniae, an anthropogenic increase of V input into rivers

and oceans may result in local toxic levels of several 10's to 1,000's µg/L of V, i.e. about one to three orders of magnitude above the natural V concentration in rivers and oceans (Smit, 2012; Schiffer and Liber, 2017a,b).

2.2 Vanadium isotope systematics

Vanadium has only one stable isotope (^{51}V), and one very long-lived radioactive isotope (^{50}V) with a half-life time of ~$1.4 \bullet 10^{15}$ years (Shore et al., 2010) which can be considered a stable isotope in isotope geochemistry. The natural $^{51}V/^{50}V$ ratio of ca. 400 is high when compared to isotope ratios of other metals like Cu, Tl, and U, but subtle V isotope variations are nevertheless resolvable with high-resolution-multi collector-inductively coupled plasma-mass spectrometry (MC-ICP-MS, e.g., Prytulak et al., 2011; Nielsen et al., 2011; Wu et al., 2016; Schuth et al., 2017). Vanadium isotope analyses face two major challenges: (i) limited control of mass interferences and instrumental mass bias because only two stable isotopes of V exist, and (ii) the requirement of high-degree V purification because of the interferences of ^{50}Cr and ^{50}Ti on the low-abundance ^{50}V. The V isotope variations are given in the delta notation as $\delta^{51}V$, i.e. the V isotope deviation of a sample from a reference standard in per mil units (‰).

Theoretical calculations suggest redox-induced V isotope fractionation of up to ~6 ‰ at 25 °C (Wu et al., 2015). First high-precision multi collector-inductively coupled plasma-mass spectrometry (MC-ICP-MS) V isotope data were reported by Nielsen et al. (2011, 2014) and Prytulak et al. (2011, 2013), who also improved the analytical procedures. These authors showed that there is a significant V isotopic difference of ca. 0.8 ‰ between bulk silicate Earth (including altered oceanic crust) and various meteorites. Recent analyses of V isotopes of Mariana island arc lavas showed a large spread of $\delta^{51}V$ for a magmatic system of about 2 ‰ (Prytulak et al., 2017). The authors conclude that V isotope fractionation is generated during fractional crystallization driven by V bonding differences between the crystallizing mineral phases and the remaining melt. A first study performing V isotope analyses on biological material investigated the V isotope signatures of the fungus Fly Agaric from different locations in Sweden and Russia (Malinovsky and Kashulin, 2016), and revealed an overall spread of ca. 2.4 ‰ with $\delta^{51}V$ values being (i) location-specific, and (ii) as high as ca. +2.3 ‰.

Furthermore, a large variation of 1.5 ‰ was observed in crude oil from different locations (Ventura et al., 2015). Interestingly, carbonate-hosted crude oils seem to have higher V concentrations and V isotope compositions up to ca. 1 ‰ higher than relatively V-poor crude oils hosted by siliciclastic host rocks. Vanadium sulfide mineral analyses of a bitumen deposit that was strongly overprinted by V-rich hydrothermal fluids revealed high $\delta^{51}V$ isotope signatures of up to +0.43 ‰ (±0.18, 2s.d., Schuth et al., 2017), whereas those of carbonate-hosted crude oils that scatter around -0.5 ‰ (Ventura et al., 2015). It is yet unclear if these locally distinct V isotope signatures are generated (i) during the deposition of the organic-rich precursor sediments, or (ii) during formation and potential overprint of the crude oil e.g. by hydrothermal activity. Alternatively, the V isotope ratios of crude oil may indicate a signature of bioactivity, hence potentially allowing the use of V isotopes as a tracer for such processes.

For modern marine settings, a significant difference of ~0.7 ‰ between two Fe-Mn nodules, NOD-A (770 µg/g V, $\delta^{51}V$ = 0.99 ‰ ±0.10, 2s.d.) and NOD-P (570 µg/g V, $\delta^{51}V$ = 1.65 ‰ ±0.06, 2s.d.), was found by Wu et al. (2016). Nodule NOD-A originated from a depth of ca. 780 m at the Blake Plateau (NW Atlantic, in the vicinity of the North-American continental shelf), and is isotopically close to altered oceanic crust, whereas nodule NOD-P is from ca. 4,300 m depth of the east Pacific Ocean and yielded the so far lowest $\delta^{51}V$ value known. This variation may indicate different V sources (e.g., continental margin derived V vs. a hydrothermal origin of V), and/or different formation conditions or processes (like water chemistry, redox conditions, adsorption). Recently, Wu et al. (2019) investigated the V isotope composition of ocean water collected at locations in the Gulf of Mexico, the North Pacific (deep water from the ALOHA station), and the North Atlantic (ca. 10 km east of Bermuda Island, and Sandy Cove, Nova Scotia, respectively). The sample material from Sandy Cove is available from the National Research Council of Canada (NRC) as the reference solution NASS-6. The authors found relatively high average $\delta^{51}V$ values for all samples ranging from +0.18 ‰ ±0.11 (2s.d., Gulf of Mexico) to +0.32 ‰ ±0.13 (2s.d., NASS-6: North Atlantic). These values overlap within analytical uncertainty, but still indicate a small variation between the sampling locations.

The highly challenging analytical requirements of V isotope measurements have been addressed only in the last few years, but because of a very limited database, the V isotope signatures of aqueous environments are still poorly understood. According to the redox

sensitivity of V and its rather long residence time in oxidized ocean water, stable V isotopes may be a powerful tool to investigate redox changes in modern oceans in detail, and be complementary to other isotope systems like Cr, Mo, and U. Once the modern V cycle and its isotope signature is better understood, it can be potentially used to elucidate in more detail past variations of the V cycle, which may be attributed to changes in the oxygen level of the early Earth's atmosphere and hydrosphere.

3 Samples

The Yangtze River is the largest river in Asia, and its numerous tributaries emerge in and pass through a geologically diverse region with magmatic, metamorphic, and sedimentary rocks covering the geological time from the Proterozoic to the present as illustrated in Fig. 2 (Saito et al., 2017). For this study, 13 water samples from the eastern Yangtze River Basin were collected in May 2017 (Table 1). Of these, 10 samples are river water samples, whereas the remaining samples include a sample from a hot spring within the city of Nanjing, water emerging from a small abandoned underground mine, and water from a stream source. The latter two samples originated within the early Cambrian Niutitang Formation which is marked by the occurrence of black shales that feature a particular enrichment in V and other metals like Ni, Mo, and U in a range of up to several 1,000 µg/g (for a detailed description of the Niutitang Formation, see e.g., Xu et al., 2012, 2013, and references therein). After a volume of at least 2.4 L per sample was collected, the river water samples were filtered completely in less than 6 hours after being taken from the sampling location through a polycarbonate filter device employing cellulose nitrate filter sheets with a pore size of 0.45 µm and a small pump operated at ca. -350 hPa (see Electronic Appendix for details). After filtration, the solution was acidified by addition of concentrated HNO_3, yielding 3 % HNO_3 in the samples. It is important to note that for this study, we define all V and Fe that has passed the 0.45 µm filters as the dissolved V and Fe load. All V and Fe that was retained by the filters, i.e. having a particle size >0.45 µm, is defined here as particulate-bound V and Fe, respectively.

A water sample with a volume of ca. 19 L from the North Sea was provided in December 2015 by the University of Oldenburg (Germany), and originates from a sampling station near the East Frisian island of Spiekeroog, north of the German coast (Table 1). The

sampling area is part of the Wadden Sea that stretches along the Dutch and German North Sea coast line. It features a shallow sea region influenced by strong tidal activity, thus significantly affecting the redox potential of ca. 9,000 km^2 of land being exposed to air and covered with water, respectively, twice per day. Investigation of trace metal dynamics of the Wadden Sea showed that the seawater is enriched in V with an average of 3.2 µg/L when compared to the average oceanic value of ca. 1.9 µg/L V given by Beck et al. (2012; V concentrations are the sum of dissolved and particulate V). Moreover, the concentration of dissolved V decreases from the coast towards the open sea, which is attributed to flocculation and precipitation of particulate matter and V adsorption to the latter (Beck et al., 2012). In addition, a strong seasonal and tidal variation of dissolved V was recognized for the Wadden Sea water (near the island of Spiekeroog) which was significantly higher in summer (ca. 2 to ca. 3.5 µg/L) than in winter (V scattering around 1.5 µg/L), and also concurrent with organic matter and bioactivity (Beck et al., 2008; Kowalski et al., 2009). The North Sea water sample for this study was taken from a storage tank at the University of Oldenburg. Because the water was already filtered and acidified shipboard to ~1 % HCl before being collected in the storage tank, no subsequent filtering was performed in order to assess the particulate load and its V isotope signature. An overview of the samples collected in the P.R. China and the German North Sea coast is given in Table 1.

As a reference material with certified V and Fe concentrations, we investigated the NASS-6 seawater (North Atlantic Surface Seawater, sampled near Sandy Cove, Canada) that is commercially available from the NRC (National Research Council of Canada), and has also been used as a reference sample by Wu et al. (2019) for V isotope investigation. This enables a direct comparison of our method of V separation from seawater to the procedure developed by these authors. The NASS-6 reference solution was filtered, UV-radiated, and acidified by the NRC Canada, as stated in its certificate.

4 Methods

In the following, we describe major points of our methods to separate V from river water, filters, and seawater matrices, and to analyze their V concentrations and isotope ratios by (MC-)ICP-MS. More details of our methods are given in the Electronic Appendix.

4.1 Vanadium concentration analyses

All water samples and filters were analyzed for their V concentration prior to V separation in order to assess if the V concentration and the sample volume (for water samples) is sufficient for later analyses via high resolution-MC-ICP-MS. A Thermo-Scientific Element XR fast-scanning high-resolution sector-field ICP-MS at the Institute for Mineralogy (University of Hannover, Germany) was employed for determination of Ti, V, Cr, and Fe concentrations in medium resolution mode to resolve molecular interferences of e.g., $^{31}P^{16}O^{+}$ (^{47}Ti), $^{35}Cl^{16}O^{+}$ (^{51}V), $^{36}Ar^{16}O^{+}$ (^{52}Cr), and $^{40}Ar^{16}O^{+}$ (^{56}Fe) (e.g., Becker and Dietze, 1998). Prior to ICP-MS analyses, aliquots of 5 mL were taken from the filtered and acidified river water samples, and doped gravimetrically with a pure Indium solution (Alfa Aesar Specpure, Germany) as an internal standard, yielding 5 µg/L of In. Pure 3 % HNO_3 doped only to contain 5 µg/L of In was used as an analytical blank. For quality control, the lake water reference solution TMDA-51.4 (fortified Lake Ontario water; obtained from Environmental Canada, Canada) was diluted gravimetrically by adding concentrated HNO_3 (from initially 0.2 % to yield 3 % HNO_3, i.e. to be at the same HNO_3 concentration as the samples and calibration solutions) and doped with the same In solution like the samples to yield 5 µg/L of In. The TMDA-51.4 solution is certified for concentrations of the above given elements (among others), and was always analyzed at the beginning and the end of a measurement session to ensure data quality.

The employed cellulose nitrate filters, including three blank filters, were placed in Savillex® Teflon beakers (90 mL), covered with 10 mL concentrated HNO_3 per filter, and kept overnight in closed beakers at 85 °C on a hot plate in a class 100 clean laboratory (see Soylak et al., 2002, for a similar method). This disintegrated the filters completely, and the solution was dried down at 105 °C. For further removal of any remaining organic compounds, the filter samples were prepared for digestion in a microwave system, as described in the Electronic Appendix. After digestion, aliquots for ICP-MS analyses via the Element XR were prepared as described above. The remaining solutions were dried and then covered with 1 M HNO_3 in preparation of the V separation protocol.

4.2 Vanadium separation from river water and filters

After the V concentrations in the river water samples and the filters were known (see results below), those samples with sufficient V contents for further V separation and multiple V isotope measurements were dried step-wise in 90 mL Teflon beakers at 105 °C until at least 500 ng of V had accumulated in the dry residue. Depending on the sample, between 0.5 and 3.3 L of acidified water were evaporated (see Table 1). As the samples represented filtered fresh water, the salt load was low when compared to seawater, allowing for dissolution of the dry residue in 5 mL of 1 M HNO_3 or less, depending on the individual sample.

Our aim to accumulate at least 500 ng V for MC-ICP-MS analyses was not possible for spring water (sample CW-7) emerging at a phosphorite-barite layer boundary in the Niutitang Formation and the hot spring water within the city of Nanjing (sample CW-12), due to very low V concentrations in these samples and insufficient sample volumes (see Table 1 and the results section). For the filters, those from sample locations CW-1, CW-2, CW-8, CW-9, CW-10, and CW-12 did not retain sufficient amounts of V for MC-ICP-MS measurements (see results). However, except for the hot spring (CW-12), all other locations allowed further investigation of the V isotope signature, either by the filter, the water, or both.

The dry river water residues were treated with aqua regia in closed Teflon beakers over night at 160 °C on a hotplate. After drying again, a further step involving concentrated HNO_3 and 10 % H_2O_2 at 105 °C was carried out over night again to remove potentially remaining organic compounds. A final drying step followed, then the sample and filter residues were dissolved in 1 M HNO_3, making them ready for the V separation procedure.

Aside from minor modifications, we adopted the V separation procedures described by Wu et al. (2016). A brief overview of the protocol is given in Fig. 3. We start the V separation of the river samples with cation resin (Bio-Rad® AG 50WX12, 200-400 mesh) that is marked as step 2 in Fig. 3 to remove most of the major elements as well as Ti, followed by anion resin (Bio-Rad® AG 1X8, 200-400 mesh) in the two column steps 3 and 4 in Fig. 3 to remove Cr and remains of other elements (like alkali metals, see also Schuth et al., 2017). The anion resin was discarded after each use, whereas the cation resin was kept in the columns, cleaned and used three times before being discardedSamples that required a volume of >1 mL 1 M HNO_3 to dissolve completely were loaded on several columns in parallel to avoid overloading of an individual column with matrix elements.

All matrix and cleaning cuts of all column steps were collected in addition to the V cuts, in order to (i) check if V was lost into the matrix or cleaning fraction, and (ii) to assess the purity of the V fractions after each separation step. For this, all collected fractions were dried at 105 °C and dissolved in 1 mL of 1 M HNO_3. Aliquots of 10 µL were diluted with 1 mL 3 % HNO_3 containing 5 µg/L of In, and analyzed via ICP-MS as described above. If more than 10 % V was found in the matrix fractions relative to the total V content (i.e. the sum of V_{Matrix} and $V_{Purified}$), the relevant cuts were combined and the separation process was repeated. This was necessary only once for the water samples CW-6 and CW-9, for which the first column step had to be repeated due to some V being eluted too early into the HF-HNO_3 (i.e. matrix) fraction. Procedural blanks were processed and analyzed for V in the same way as the samples. The total blank contribution of V was always found to be lower than 0.5 ng, which is negligible relative to the V concentration of at least 500 ng in our purified V fractions. The same is true for the blank filters, where no V could be detected at all.

In accordance with the findings of Wu et al. (2016), the cation column step removed already large quantities of major and trace elements (e.g., Na, Ca, Mg, Al, K, Ti, Fe, Cr). This allowed merging of several V fractions of the same sample prior to the following purification step employing anion resin, i.e. samples which were initially split and then loaded onto more than one cation resin column. The final purification step employing the micro columns was typically performed two to three times to ensure V fractions that were devoid of Cr, Ti, but also of Ca and Zn, which occasionally were found to be present at similar or higher concentrations than V after passing the micro-columns for the first time. The total V recovery after all purification steps was ≥90 %, not including the removal of small V quantities (typically 1 % of total V) for ICP-MS analyses between the purification steps.

4.3 Vanadium separation from seawater

Wu et al. (2019) developed a multi-column procedure to separate V from seawater samples. When compared to their earlier method for V separation from e.g. rock samples (see Wu et al., 2016), they replaced their cation resin PP column with a quartz glass column filled with quartz wool and Nobias PA-1 resin (available from Hitachi High-Technologies, Japan). This resin was used to retain V and other metals, while the alkalis and alkali earth metals are washed out (Sohrin et al., 2008). Per column, Wu et al. (2019) did not load more

than 250 mL of seawater that was adjusted to pH=6 (±0.1) and buffered with ammonia-acetate. Vanadium was then eluted with 3 M HNO_3. To process larger amounts of a seawater sample, the authors cleaned the resin and conditioned it again for the next load of seawater. The accumulated V fraction was then subsequently purified by procedures similar to those employed for e.g. rock samples, i.e. using anion resin to separate V from remaining matrix elements like Cr and Ti (see Wu et al., 2016, 2019, for details of the different methods).

In an alternative approach, we decided to use Bio-Rad® Chelex-100 resin (1 % cross-linkage, 100-200 mesh, Na^+ form) that was used successfully already in earlier studies for V separation from seawater samples (Abbasse et al., 2002; Wang and Sañudo Wilhelmy, 2008). The Chelex-100 resin can serve, as the Nobias PA-1 resin, as an efficient chelator due to its iminodiacetic acid functional groups for many metals but not for the salt matrix of seawater. We adopted the method described earlier by Abbasse et al. (2002) who investigated V concentrations in seawater samples. Prior to use, new resin was cleaned according to Table S1 in the Electronic Appendix. To chelate V effectively, the resin must be converted from the H^+ form that is produced during the cleaning step to the NH_4^+ form by passing 1 M NH_3 through the resin. Excess ammonia was subsequently rinsed with water. The resin was then stored in a LDPE bottle in 1 M ammonium-acetate buffer solution at pH=5 prepared from 25 % NH_3 and 100 % acetic acid. The V separation procedure for seawater samples is illustrated in Fig. 3.

In step 1 in Fig. 3, a volume of ca. 5 mL of the prepared Chelex-100 resin was loaded into a PP column mounted onto 2 L pre-cleaned LDPE bottles, in which the matrix solution was collected for later investigation by ICP-MS and tests involving doping with a V standard solution (see Fig. 4). Immediately prior to loading of the sample solutions, the pH of the acidified seawater samples was increased by a step-wise addition of 25 % NH_3 to pH=5 (±0.1). The increase of pH was controlled in regularly taken aliquots of 2 mL with a Mettler-Toledo FG2 instrument. Fresh pH standard solutions (Thermo-Scientific, Germany) at pH=4 and pH=7, respectively, were used to calibrate the pH analyzer immediately before use. To buffer the sample pH during the V separation procedure, 35-50 mL of 1 M ammonium-acetate solution were added to each sample volume (2 L). A blank solution of 2 L of purified water but otherwise acidified to 1 % HCl and then adjusted to pH=5 was prepared as well. The North Sea sample was split in several 2 L LDPE bottles to be processed in parallel and serve as a control of reproducibility. A 4-channel peristaltic pump (Cole-Parmer Masterflex

L/S, USA) equipped with Tygon tubes (1.52 mm inner diameter, type LMT-55; pre-cleaned with 3 % HNO_3 overnight, then rinsed with water, and finally conditioned with the ammonia-acetate buffer solution) was used to pump the sample solutions at a drop rate of ca. 1-2 mL/min onto the resin. After the full sample volumes had passed the resin, the columns were transferred into a plastic rack, and the remaining salt matrix was eluted and collected with 30 mL of 0.5 M ammonium-acetate buffer solution at pH=5. Vanadium and other metals (e.g., like Fe, Cr, and U) are marked by a light brownish coloration at the top of the resin and were subsequently eluted with 40 mL 2 M HNO_3/0.5 M HCl. Notably, the Chelex-100 resin is pH-sensitive in a way that it shrinks within seconds by more than 50 % from its volume in NH_4^+ form when covered with acid. This effect is reversible (i.e., the resin expands at higher pH), and may be used as a qualitative indicator of the pH condition during V separation. After elution of the V fraction, the resin was cleaned with 80 mL 2 M HNO_3/0.5 M HCl, 3 cv of water, 80 mL 2 M NH_3, and 3 cv of 1 M ammonium-acetate buffer. Each of these solutions were collected separately for later investigation via ICP-MS. To process these large amounts of solutions in a timely manner, tight-sealing PP funnels (type R1030, Rockbourne Scientific, UK) were mounted on the columns. The resin was removed from the columns afterwards and stored again in the buffer solution.

The matrix fractions, the V fraction, and the cleaning solutions after V collection were dried at 105 °C, and covered with aqua regia to remove a potential resin contribution, before drying them again. The V recovery was investigated by dissolving the dry residues in 1 M HNO_3, of which aliquots were diluted to 3 % HNO_3 and doped with 5 µg/L In for ICP-MS analyses. Subsequently, the V fractions were purified further by steps 2 to 4 as illustrated in Fig. 3. The V purification steps for the NASS-6 sample were identical to the column steps 1 to 4 (micro-column) described in Fig. 3. For the North Sea samples, Ti was removed by dissolving the sample in 6 M HCl and passing it through LN resin (Triskem, France) in a micro-column as described earlier by Schuth et al. (2017). As for the other cleaning steps, the matrix of the LN resin cleaning procedure was collected and analyzed by ICP-MS. Subsequently, the North Sea V fraction was dried, treated with aqua regia and loaded onto Bio-Rad® AG1X8 anion resin for a final purification of the V cut.

To test our method employing the Chelex-100 resin and the purification steps afterwards for consistency and V recovery, we collected the water of the North Sea samples and the NASS-6 solution after it has passed the Chelex-100 resin. Aliquots of these solutions

were doped gravimetrically to yield 5 µg/L of In and analyzed with the Element XR ICP-MS for potential traces of V. After passing the Chelex-100 resin the V content of the NASS-6 reference material was below the detection limit. The North Sea aqueous matrices were then doped with a pure Alfa Aesar and a NIST-3165 V solution, respectively, to yield 5 µg/L of V. These samples were then processed again in the same way as the original sample solutions (Fig. 3).

All processed samples were considered suitable for V isotope analyses via MC-ICP-MS if no Cr and Ti could be detected in the aliquots of the purified V fractions by ICP-MS measurements.

4.4 Vanadium isotope analyses

We used both the Thermo-Finnigan Neptune and the newer Thermo-Scientific Neptune *Plus* high resolution-MC-ICP mass spectrometers at the Institute for Mineralogy (University of Hannover) for V isotope analyses. The Neptune *Plus* was used to analyze all water samples, and set to the detector configuration described by Schuth et al. (2017) to cover the mass range from ^{49}Ti to ^{57}Fe (see Table 3). The older Neptune instrument was used for filter and replicate water analyses, but it lacks the additional L5 detector and covers the masses from ^{49}Ti to ^{56}Fe instead as shown in Table S-2 in the Electronic Appendix. The detectors were connected to 10^{11} Ω amplifier resistors, except the detector assigned to ^{51}V which was connected to a 10^{10} Ω resistor due to signal intensities >45 V. The instruments were set to high-resolution mode (providing a resolving power of ~10,000 for Δm/m, with Δm calculated at 5% and 95% signal intensity) to resolve interferences like $^{36}Ar^{14}N^+$ ($^{50}V^+$), $^{35}Cl^{16}O^+$ ($^{51}V^+$), $^{36}Ar^{16}O^+$ ($^{52}Cr^+$), $^{40}Ar^{14}N^+$ ($^{54}Fe^+$), $^{40}Ar^{16}O^+$ ($^{56}Fe^+$), and $^{40}Ar^{16}OH^+$ ($^{57}Fe^+$) on the masses of interest (Weyer and Schwieters, 2003; Nielsen et al., 2016; Wu et al., 2016). We used an Aridus-II (CETAC Technologies, USA) desolvating device equipped with a PFA nebulizer for dry plasma conditions, which is similar to the analytical setup of Wu et al. (2019). However, in contrast to these authors who used a jet sample cone, we installed a conventional Ni sample cone, because high Ar-N formation rates in our mass spectrometers exceeded a signal intensity of 50 V (for $^{40}Ar^{14}N^+$) when employing a jet-type sample cone. Such high Ar-N signals decreased the widths of the ^{50}V and ^{54}Fe plateaus when compared to a conventional sample cone.

For correction of instrumental mass bias, all samples and standards were matched to similar V concentrations within a ±10 % tolerance in 3 % HNO_3. They were furthermore doped with Fe that was prepared from the Fe isotope reference material IRMM-014 (purchased from the Institute of Reference Materials and Measurements; Geel, Belgium) to yield ca. 20 V signal intensity for ^{56}Fe with certified $^{56}Fe/^{54}Fe$ of 15.698 and $^{57}Fe/^{56}Fe$ of 0.02309. These ratios were then used to calculate the mass fractionation factor β_{Fe} in the exponential law to correct for instrumental mass fractionation (see Schuth et al., 2017). As demonstrated already for $^{51}V/^{50}V$ measurements of minerals via laser ablation-high resolution-MC-ICP-MS by Schuth et al. (2017), this approach of mass bias correction has little effect on the accuracy and precision of $^{51}V/^{50}V$ alone, but it results in a much more accurate interference correction of the ^{50}V signal for the ^{50}Cr and ^{50}Ti contributions because it takes potential variations of the individual sample matrix compositions and instrumental drift into account. For correction of these mass interferences on ^{50}V, we measured the intensities of ^{52}Cr and ^{49}Ti and applied the mass fractionation factor β_{Fe} to the natural ratio of 0.051856 for $^{50}Cr/^{52}Cr$ (Berglund and Wieser, 2011) and 0.972537 for $^{50}Ti/^{49}Ti$ (Leya et al., 2007), respectively. Our approach of employing β_{Fe} for a mass bias corrected interference correction is different to the one described by Wu et al. (2019) who determined the mass fractionation factors β for Cr and Ti, respectively, for pure Cr and Ti solutions at the beginning of their analytical sessions, and used these constant β_{Cr} and β_{Ti} values to correct the ^{50}V signal in their samples for Cr and Ti contributions.

The high resolution mode, the conventional cone assembly, and a slower solution uptake rate (Table S-2, Electronic Appendix) employed in our study resulted in a signal intensity of ~100-150 V/ppm, which is somewhat lower than the ~150-250 V/ppm reported by Wu et al. (2019). A major advantage of our setup, however, is the possibility to analyze each sample for a longer time individually, and also perform in most cases three repetitive measurements per sample to achieve reliable analytical reproducibility. Each sample analysis comprises 25 measurement cycles of 4.194 s per cycle in static mode. Every sample measurement was bracketed by analyses of a V reference solution. In our study we calculate the $\delta^{51}V$ values against the average result of the NIST-3165 vanadium reference material from the National Institute of Standards (NIST, Gaithersburg, Maryland, USA) measured before and after each individual sample according to equation 1:

$$\delta^{51}V_{NIST} = \left(\frac{(^{50}V/^{51}V)_{sample}}{(^{50}V/^{51}V)_{Nist-3156}} - 1 \right) \cdot 1000 \qquad [‰] \quad \text{(eqn. 1)}$$

This can be converted to the $\delta^{51}V_{AA}$ values that are reported in several other studies, where the in-house Oxford Alfa Aesar vanadium solution (V_{AA}) was employed as a reference standard (Prytulak et al., 2011; Nielsen et al., 2011), by equation 2:

$$\delta^{51}V_{AA} = \delta^{51}V_{Sample/NIST} - \delta^{51}V_{NIST/AA} \qquad [‰] \quad \text{(eqn. 2)}$$

We like to emphasize that pure V solutions provided by Alfa Aesar in various countries use V from different sources and/or apply different purification procedures, which result in different V isotope signatures of three Alfa Aesar solutions of different age and origin (see Schuth et al., 2017, for discussion). Hence, we decided to use a the NIST-3165 vanadium solution as a reference which is controlled for chemical composition and prepared by the National Institute of Standards and Technologies (NIST) that provides a wide range of elemental and isotopic reference materials. To allow an easy comparison of $\delta^{51}V$ values from other studies who often refer to the Oxford V_{AA} solution first employed by Prytulak et al. (2011) and Nielsen et al. (2011), we also measured the V isotope composition of the BDH solution (from BDH Chemicals, UK, provided by J. Prytulak; see Prytulak et al., 2011, Nielsen et al., 2011) against the Oxford V_{AA} solution several times per analytical session. The BDH solution has been used in all V isotope studies so far as an in-house standard and is therefore well known (Prytulak et al., 2011; Nielsen et al., 2011, 2016; Schuth et al., 2017; Wu et al., 2016, 2019). The average $\delta^{51}V_{AA}$ of the BDH solution in our study is -1.22 ‰ (± 0.12, 2s.d., n=11), which is in perfect agreement of earlier results (see references above) and proves that our analytical method is reliable and precise. Against NIST-3165, the Oxford V_{AA} solution gives an average value for $\delta^{51}V_{NIST}$ = -0.61 ‰ (±0.13, 2s.d., n=10), and is therefore in good concordance with the value of -0.67 ‰ (±0.07, 2s.d., n=4) given by Schuth et al. (2017). For convenience and better comparison with previously published stable V isotope data, we will discuss our results in the following as $\delta^{51}V_{AA}$ values, although all results are presented both as $\delta^{51}V_{NIST}$ and $\delta^{51}V_{AA}$.

4.5 Vanadium purification efficiency

The 3-column vanadium purification procedure adopted from Wu et al. (2016) for the river water and filter samples was controlled after each purification step via ICP-MS measurements. The method is reliable and efficient with recovery rates of at least 95% for V even after repetitive purification steps, and thus can be well adapted also for river water samples. Multiple re-uses of the cation resin in the first V purification step have no negative effect on its V retention capability or the V blank level. Nevertheless, we discarded the cation resin after three uses without investigating its potential life time further.

The Bio-Rad® Chelex-100 resin is, as the Nobias PA-1 resin employed by Wu et al. (2019), an efficient chelator for V (see also Abbasse et al., 2002; Wang and Sañudo Wilhelmy, 2008). In contrast to the approach described by Wu et al. (2019) who confined to a loading limit of 250 mL solution per column filled with 1.5 mL Nobias resin to achieve a V recovery of ca. 70 to 75 % for the NASS-6 reference solution and other seawater samples, we found that ca. 5 mL of Chelex-100 resin used per column were able to retain ca. 95 % of the V fraction even when loaded with 1 L of the NASS-6 reference solution. Similar high retention rates of V from seawater were also reported by Abbasse et al. (2002) for the Chelex-100 resin. There are a couple of reasons that may explain the higher recovery rate even at a higher sample load found for the NASS-6 reference material after passing the Chelex-100 resin:

1. We loaded the solution drop-wise via a peristaltic pump onto the Chelex-100 resin, thus allowing a slow flow of the solution. This may have supported a more efficient metal adsorption. A large volume of solution would pass faster through the column due to gravity, and thus some V may not be adsorbed to the resin.
2. The Nobias PA-1 resin employed by Wu et al. (2019) may not be as efficient as the Chelex-100 resin to retain dissolved V, simply because the two methods work at different pH conditions, i.e. at pH=6 (Wu et al., 2019) vs. pH=5 (our study). Gustafsson (2019, and references therein) discusses that pH=6 is a "switching" point, i.e. dissolved V that would be present at pH ≥6 as a tetrahedral vanadate ($H_nV^{V}O_4^{(3-n)-}$) can be easily reduced to its vanadyl species $V^{IV}O^{2+}$ at pH <6 by organic acids like oxalic acid or other organic compounds with carboxyl groups, e.g., like acetic acid which is present in the buffer solution used in both studies (e.g., Bruyère et al., 2001). Vanadyl is known to form strong bonds with organic

606 ligands (e.g., Kowalski et al., 2009; Wang and Sañudo-Wilhelmy, 2008, 2009;
607 Gustafsson, 2019), and thus may be better retained on the resin at pH=5.
608 Yet it remains to be investigated if a lower pH and/or slower flow rate of the sample
609 solution has a significant effect on the V retention capability of the Nobias PA-1 resin.
610
611 When processing our North Sea water samples through the Chelex-100 resin, the V
612 recovery dropped to ca. 70 - 80 %, and is thus on the same level as described by Wu et al.
613 (2019) for the seawater samples of their study. The North Sea water was acidified to ca. 1 %
614 HCl but otherwise no effort was made to destroy potentially present metal-organic
615 complexes which is in contrast to UV radiation of the NASS-6 reference solution. The
616 similarly reduced V recovery for non-irradiated seawater of the two studies support the
617 assumption of Wu et al. (2019) that organic complexes may partially inhibit V adsorption to
618 the resin. To test our method further, the North Sea water was collected in five separate
619 bottles after it had passed the Chelex-100 resin for the first time, and subsequently acidified
620 again to 1 % HCl. The water in these bottles was then doped either with an Alfa Aesar or the
621 NIST-3165 solution (see Table 2), to yield 5 µg/L of V, then brought to pH=5, and passed
622 again through the purification procedure, starting with the Chelex-100 resin (Fig. 3). As
623 before, the V recovery was lower than in comparison with the NASS-6 solution but not as
624 much as for the natural samples, and ranged between ca. 76 to 87% for the solution doped
625 with NIST-3165, and ca. 92 to 97 % for the solution doped with Alfa Aesar. Supposedly either
626 the amount of organic ligands was reduced during the previous removal of natural V, thus
627 increasing the amount of doped V available for chelation by the resin, or the added V was
628 not yet complexed efficiently by the natural organic compounds still present in the solution.
629 Still, the V signatures of the doped seawater solutions were reproduced within analytical
630 uncertainty, albeit at a tendency towards $\delta^{51}V$ values slightly lower than 0 ‰ with -0.11 ‰
631 (±0.19, 2s.d., n=11) for NIST-3165 and -0.17 ‰ (±0.23, 2s.d., n=10) for Alfa Aesar (Table 4).
632 This effect can also be observed in a weaker occurrence in the data reported by Wu et al.
633 (2019). They, however, doped their natural seawater samples without removing its natural V
634 fraction beforehand in a series of experiments with synthetic Alfa Aesar at much higher V
635 concentrations of 10 µg and 25 µg per 250 mL, respectively, and observed recovery rates of
636 87 to 105 %.

In conclusion, our study showed that the procedures developed for V separation from seawater are giving reproducible V isotope results and also tolerate reduced yields of ~75 % without incurring a significant V isotope fractionation during the purification process.

5 Results and discussion

The results of the V concentration and isotope measurements by high resolution (MC-)ICP-MS are given in Table 4. Please note that the isotope data are given both as $\delta^{51}V_{NIST}$ and $\delta^{51}V_{AA}$, with the latter being referred to in the discussion. In the following text, the dissolved V and Fe concentration refers to the filtered solution (< 0.45 µm), and particulate V and Fe refers to the V and Fe concentrations in material retained by the filters (> 0.45 µm).

5.1 Vanadium concentrations

Most of the river water samples have typically low dissolved V concentrations with an average of ~0.8 µg/L for our sample suite, in accordance with the average of ca. 0.7 µg/L given e.g. by Huang et al. (2015) and Shiller and Boyle (1987). The particulate V fraction varies between the sample locations, but is typically up to one order of magnitude lower than the fraction of dissolved V. An exception is seen for the sample CW-3 from the abandoned mine, where the highest load of particulate V occurred with 17.5 µg/L (FCW-3). While there is a considerable variation of the dissolved V concentration in the sampled rivers ranging from ca. 0.07 to 6 µg/L in our sample suite, an overall increase of the V concentration from small tributaries to the Yangtze River as the major water body can be observed. Moreover, for the Yangtze River a gradual increase of particulate-bound V and Fe was seen between the Three-Gorges-Dam and the city of Nanjing.

5.1.1 Vanadium in river source, hot spring, and mine effluent waters

There are some notable extreme V concentration results in our study that support different processes controlling the V abundance in water bodies: (i) sample CW-3 (effluent of an abandoned underground uranium mine) features V concentrations three times higher than in the Yangtze River and is also rich in U (130 µg/L, not shown in Tab. 4), and (ii) sample CW-12 (hot spring water in Nanjing) is almost devoid of V and other trace metals. The filters

of CW-3 and CW-12 mimic this finding, with extremely high and low loads of V, respectively (17.5 µg/L, and below detection limit, respectively, Table 2). For the hot spring water sample CW-12, the absence of V is not surprising because dissolved V is scavenged efficiently by precipitation of Fe oxides and adsorption as shown for mid-ocean ridge settings before it enters the open water body (e.g., Trefry and Metz, 1989; German et al., 1991). Consequently, sample CW-12 and its filter were not considered for further investigation of V isotope signatures. In contrast to this V-poor sample, the high V and U concentrations of sample CW-3 are probably related to V-rich black shales within the Niutitang Formation (Xu et al., 2012), which are abundant in the sampling area. Former underground mining activities most likely have exposed more V-rich material to water and atmospheric oxygen than in an undisturbed natural setting, thereby facilitating oxidation and concomitant efficient mobilization of V and U. In contrast to the V-rich water released from the black shales at CW-3, little dissolved V was found in a small spring emerging between phosphorite and barite layers of the Niutitang Formation (sample CW-7). However, the filter of this sample (FCW-7) revealed more than two times higher V (and three orders of magnitude higher Fe) concentrations, a feature that is visible also for sample CW-3 and FCW-3, but at a much higher absolute V concentration for the latter (Table 2). This suggests that particulate V transport at least for these two water sources (CW-3, CW-7) is the dominant process. For the spring water of CW-7, either (i) the dissolvable V pool accessible to groundwater is already exhausted, (ii) the V concentration in the sampling area is overall low because the phosphorite layers did not form at euxinic conditions (thereby less V was immobilized in these layers ab initio), or (iii) the redox conditions at that location are low and thus not favoring V mobilization (cf. Wright et al., 2014). Highly variable V concentrations of ca. 270 to 4,400 µg/g are known for the Niutitang Formation, but a rather low V abundance of ~420 µg/g was reported for phosphorite layers (Xu et al., 2012). This supports the assumption that a low V pool can be present in the rocks at the spring of CW-7.

5.1.2 Vanadium in tributary rivers

The dissolved V concentrations in the sampled tributary rivers to the Yangtze River are typically low, and scatter between ca. 0.2 (CW-5) to 1.1 µg/L of V (CW-4). Vanadium amounts retained by the filters are often lower by factors between 3 and 10 relative to the dissolved V fraction. Noteworthy are the absolute elevated amounts of particulate V and Fe

in filter samples FCW-4, FCW-5, and FCW-6. The first two were collected from fast-flowing, but small rivers in a sparsely populated region, and their V budget may be attributed to particles eroded from country rock, or represent plant litter, soil particles, or dust (e.g., Schlesinger et al., 2017), and are carried because of the higher kinetic energy of the water. Sample FCW-6 was collected from the large Wuyang River in the city center of Yuping. It is unclear if the elevated amount of particulate V is related to a geogenic source, or may be related to an anthropogenic source like industry, or waste water. It is however obvious from the lower V concentration in the sampled tributary rivers relative to the respective higher V concentrations in the Yangtze River that (i) they deliver only a part of the Yangtze River's V budget, and (ii) mixing processes of different water masses may dilute or modify the individual V signatures, depending on the particulate and the dissolved V load. However, an unknown amount of particulate and dissolved V is removed by sedimentation processes in the river bed as well, and may also exert some control of the overall V contribution of smaller tributaries to the large rivers.

5.1.3 Vanadium in the Yangtze River

The Yangtze River samples (CW-10, CW-11, CW-13) have the overall highest dissolved V concentrations in our study (not considering sample CW-3, see above), with variable Cr and Fe concentrations. Samples CW-11 and CW-13 were taken from flowing river water downstream of the Three-Gorges-Dam, and are marked by a high Fe (oxyhydr-)oxide particulate load as is evident from the highest Fe concentrations of the filter material in our study. Sample CW-10 was collected in the Three-Gorges-Dam lake, which represents a rather stagnant water pool. The dissolved V concentrations of CW-10 (1.6 µg/L) were slightly lower than in CW-11 and CW-13 (1.7 µg/L), but the Fe concentrations measured in the filter of FCW-10 were lower by almost one order of magnitude when compared to the filters FCW-11 and FCW-13. Adsorption to particulate matter seems to be one process that may have decreased the dissolved V fraction in the Three-Gorges-Dam lake. We assume that because of the near-stagnant surface water in the dam lake, particulate matter like Fe (oxyhydr-)oxides can settle and may act to some degree as a sorbent for dissolved V (Brinza et al., 2008; Gustafsson, 2019). However, as Fe decreased more drastically than V in the dam lake water, the effect of adsorption seems to be less significant for V, either because V can form as vanadyl (V^{IV}) strong complexes with e.g. organic matter even at oxic conditions (e.g.,

Templeton and Chasteen, 1980; Lu et al., 1998; Gustafsson et al., 2007), making it partly unavailable for adsorption to Fe oxides, or because efficient water mixing is not occurring in the dam lake and thus particulate Fe (oxyhydr)oxides are partly settling at the lake bottom. Notably, the particulate V fraction of FCW-10 is significantly lower by almost an order of magnitude when compared to FCW-11 and FCW-13. Therefore, the V load in stagnant or poorly mixed water bodies does not seem to be controlled exclusively by particulate Fe oxides, but perhaps also by metal-organic complexes that can pass 0.45 µm filters. A similar conclusion can be drawn from the results of the other Yangtze River samples. The dissolved V concentration in these samples is almost identical at 1.7 µg/L and independent of the amount of particulate Fe. The latter increases by a factor of almost 2 between the sampling locations near the cities of Wuhan (FCW-11) and Nanjing (FCW-13). An increase of ca. 35 % of particulate-bound V is however evident from filter FCW-11 to filter FCW-13. One reason for this can be a tributary river with a higher particulate load, or an anthropogenic source, e.g. from industrial facilities that are abundant along the lower Yangtze River and its tributaries. For example, an increase of trace metals due to human activity has been recorded in sediments of the Yangtze River around Wuhan for As, Cd, Cr, Cu, Hg, Ni, Pb, and Zn (Wang et al., 2011).

If a V isotope signature can be produced by human activity, i.e. by industrial-chemical processes that require V in significant amounts and subsequently release V into the environments through waste water, it can potentially be used as a fingerprint tool and sensitive tracer of V uptake e.g. in aquatic organisms. One potential example for this are corals of the South China Sea, that have archived trace metal variations of Mn, Cu, and V of the last ca. 150 years. Decadal variations of V from ca. 35 to 65 ng/g with occasional V concentration excursions in the corals of up to ca. 100 ng/g were observed (Chen et al., 2015). These variations were interpreted as a complex interplay between higher riverine V input potentially due to human activity in the ocean until 1990, and an upwelling of nutrient- and V-rich deeper ocean water (Chen et al., 2015). However, V isotope signatures by bioactivity in marine settings need yet to be investigated.

5.2 Vanadium isotope signatures

From other redox-sensitive elements, e.g. like Fe, it is now well known that processes like dissolution and precipitation (both resulting from pH and/or redox variations), and adsorption in low-temperature environments are often inducing mass-dependent isotope fractionation (see e.g. the review by Johnson et al., 2008, for Fe). Theoretical investigations by Wu et al. (2015) and the growing data set of $\delta^{51}V$ values of various matrices suggest that these processes can have a similar effect for stable V isotope compositions in the range of several per mil at environmental temperatures. For example, Wu et al. (2015) calculated a theoretical V isotope fractionation factor for V adsorption in the vanadate - goethite system with $\Delta^{51}V_{V(V)\text{-goethite}}$=2.1 ‰ (±0.4, 2s.d.), i.e. the goethite surface would be preferentially enriched in the light ^{50}V isotope due to adsorption. For an aqueous system like a river, this would result in an isotopically heavy dissolved V pool, while the adsorbed V fraction is concomitantly enriched in ^{50}V. Consequently, the presence of particulate Fe (oxyhydr)oxides as potential V adsorbers in rivers can modify the dissolved V isotope signature from its original host-rock composition at the source to higher $\delta^{51}V$ values at the river's estuary or its inflow into a larger river.

In an alternative scenario, a mixture of different V pools with distinct V isotope compositions may result in an isotope signature that is not clearly related e.g. to a host rock, but may instead indicate a biological or anthropogenic component in river waters.

For biological V isotope signatures, Malinovsky and Kashulin (2016) found for the fungus Fly Agaric (*Amanita Muscaria*) a wide range of 2.4 ‰ for the $\delta^{51}V$ values, with the highest $\delta^{51}V_{AA}$ value as high as +2.3 ‰ (recalculated from $\delta^{51}V_{NIST}$ values given by Malinovsky and Kashulin, 2016, according to eqn. 2 and assuming $\delta^{51}V_{NIST/AA}$ = +0.61 ‰). These values were found to be distinct for the fungi populations at specific locations, and thus allow tracing of the potential origin of these fungi by their V isotope signature. Consequently, such high $\delta^{51}V$ values are possible in biological material. Crude oils from various locations feature low and distinct $\delta^{51}V_{AA}$ values ranging from ca. -1.6 ‰ to -0.2 ‰ (Ventura et al., 2015). Yet it is unclear if these $\delta^{51}V_{AA}$ values are indicative of bioactivity or have been already modified by diagenesis during oil formation. Nevertheless, crude oil contains variable amounts of V (ca. 100 to 400 µg/g; e.g., Schlesinger et al., 2017), that enters ultimately the environment as aerosols by fuel combustion in power plants and cars at a rate of 100 to 280 Gg/a (Schlesinger et al., 2017). It is however unknown if oil refinement and/or combustion already fractionates the original V isotope signature of crude oil. The same may be true for V that is

796 also vastly used as a catalyst for the production of sulfuric acid by the chemical industry
797 (e.g., Lapina et al., 1999). For industrially purified V, refined V metal analyzed by Schuth et al.
798 (2017) featured a high $\delta^{51}V_{AA}$ value of +1.38 ‰ (±0.07, 2s.d., n=10), hence suggesting that
799 such high values outside the range observed for natural V hosts can indeed be produced by
800 refinement processes.
801 In the following, possible factors of V isotope modification - V adsorption,
802 anthropogenic V sources - will be discussed together with potential host rock V isotope
803 signatures for the rivers of the Yangtze River Basin.
804
805 *5.2.1 Vanadium isotope signatures of river waters*
806 The river water samples of the Yangtze River Basin show a range of dissolved $\delta^{51}V_{AA}$
807 values from -0.79 ‰ (±0.18, 2s.d.) to -0.13 ‰ (±0.22, 2s.d.) at a comparatively large spread
808 of dissolved V concentrations as illustrated in Fig. 5a. Interestingly this range is made up by
809 the three samples from the Yangtze River, with the lowest value referring to water from the
810 Three-Gorges-Dam lake, and the highest value obtained for water collected in Nanjing, i.e.
811 less than 300 km upstream of the Yangtze River estuary. The dissolved $\delta^{51}V_{AA}$ value of -0.63
812 ‰ (±0.08, 2s.d.) for V and U rich source water emerging from the abandoned mine is within
813 the range of Si-rich rocks reported by Wu et al. (2016). The dissolved V isotope signatures of
814 the small and larger tributary rivers show some variations, but however, they overlap the
815 range defined by the Yangtze River, with values from -0.76 ‰ (±0.20, 2s.d.) to -0.31 ‰
816 (±0.21, 2s.d.). In addition, they have $\delta^{51}V_{AA}$ values that overlap those of quartz-latite (-0.60
817 ‰ ±0.07, 2s.d.) and andesitic rocks (-0.70 ‰ ±0.10 to -0.80 ‰ ±0.07, 2s.d.; rock data from
818 Wu et al., 2016).
819 The V isotope compositions of the particulate V loads are, except for the extreme
820 case of sample FCW-3, all significantly lower than those of the dissolved V pool, and feature
821 a large range of variation of 2 ‰ (Fig. 5a) between -0.14 ‰ (FCW-3, abandoned mine) to -
822 2.16 ‰ (FCW-5, small and fast flowing creek water). However, excluding the two most
823 extreme values, the V isotope compositions of the other filters are confined to a narrower
824 $\delta^{51}V_{AA}$ range between -1.08 and -1.56 ‰. This range of values is lower than variations
825 observed among basalts and altered oceanic crust (ca. -0.9 ‰, e.g., Prytulak et al., 2013), but
826 overlaps the range defined by two Fe-Mn crusts (ca. -1.0 to -1.7 ‰; Wu et al., 2016). We
827 interpret the low $\delta^{51}V_{AA}$ values of particulate-bound V as a result of V isotope fractionation

828 due to adsorption (Wu et al., 2015), and furthermore assume that this process can also
829 explain the low $\delta^{51}V_{AA}$ signatures of the Fe-Mn nodules investigated by Wu et al. (2016).
830 Samples for which both the dissolved and the particulate V isotope composition have
831 been analyzed allow to calculate the total $\delta^{51}V$ value of the sample according to equation 3:
832
833 $$\delta^{51}V_{Total} = \left(\frac{V_{dissolved}}{V_{Total}} \cdot \delta^{51}V_{dissolved}\right) + \left(\frac{V_{particulate}}{V_{Total}} \cdot \delta^{51}V_{particulate}\right) \quad [‰] \quad \text{(eqn. 3)}$$
834
835 with $V_{dissolved}$ and $V_{particulate}$ being the V concentrations in the dissolved V and particulate V
836 pool, respectively (see Table 2, $V_{particulate}$ has been recalculated to the solution volume before
837 being used in eqn. 3). This results in most cases in $\delta^{51}V$ values that are plotting close to the
838 field of the average continental crust, as is illustrated in Fig. 5b. Exceptions are the V-rich
839 water from the abandoned mine (CW-3), the tributary Fe-rich and V-poor river Pingtu (CW-
840 5), and the lower Yangtze River at Nanjing (high Fe and V concentrations, Table 2), which
841 plot either above the average crustal signature, or are close to a signature found for Fe-Mn
842 nodules (CW-5, cf. Wu et al., 2016).
843
844 *Mine effluent and stream source waters* - The V isotope composition of the dissolved
845 and particulate V pools in the mine effluent and the river source water samples is very
846 diverse. For the mine water (CW-3) the difference between dissolved V (-0.63 ‰ ±0.08) and
847 particulate V (-0.14 ‰ ±0.11) is, when compared to the other samples, relatively small. Also,
848 this sample is exceptional in our suite in that it has (i) a higher particulate V load than a
849 dissolved V concentration, and (ii) more Fe is present in dissolved than in particulate form
850 (Table 2). This hints to conditions that are more favorable of mobilizing Fe rather than V in
851 dissolved form, which would be the case at low E_h (e.g. Nriagu, 1998). Consequently,
852 assuming little amounts of Fe oxides that are present to act as potential adsorbents, the light
853 V isotopes are released preferentially from the host rock because of lower bonding strengths
854 in their mineral host phases, yielding a lower $\delta^{51}V$ signature in the dissolved V fraction. The
855 higher $\delta^{51}V$ values for the particulate V have likely been depleted in the light V isotope
856 inventory during V mobilization due to a slightly weaker bonding of ^{50}V in its solid host
857 phases (see also Prytulak et al., 2017, for discussion).
858 The low particulate $\delta^{51}V$ value of -1.52 ‰ (±0.18) of the source water sample FCW-7
859 from the Phosphorite Unit in the Niutitang Formation is most likely the result of a similar

process as described for FCW-3. The V isotope composition of a sample from the phosphorite layer has been analyzed by Brüske et al. (2015) with a $\delta^{51}V_{AA}$ of ca. -1.2 ‰. This sample was however taken at a different location than FCW-7 but is of the same stratigraphic age, and its reference to the host rock of the water source of this study needs to be taken with caution. The dissolved Fe concentration in the source water (ca. 40 µg/L) is significantly lower than at CW-3, but still about one order of magnitude higher than for the other rivers. We assume that reducing conditions persist in the groundwater reservoir of the source, thereby promoting mobilization of Fe, but inhibiting release of dissolved V at the same time. This also offers an explanation for the very low dissolved V concentration in the source water.

Tributary rivers - The very low $\delta^{51}V$ value of -2.2 ‰ (±0.3) of the particulate-bound V of sample FCW-5 (Pingtu, a fast-flowing river) coincides with its low $\delta^{51}V_{AA}$ signature of -0.76 ‰ (±0.20) in the dissolved V pool (only the Three-Gorges-Dam lake has - within analytical uncertainty - a slightly lower delta value). The total V concentration of this sample is also low as well and has similar dissolved and particulate V concentrations. The particulate Fe concentration of FCW-5 is comparatively high, and only surpassed by the lower Yangtze River samples (and the rather extreme case of FCW-3, Table 2). Since the continental crust has a much higher $\delta^{51}V$ value (scattering around -0.6 ‰; Wu et al., 2016), we assume that the V isotope composition of this sample is linked to the presence of particulate Fe oxides that preferentially adsorb ^{50}V (Wu et al., 2015), and have been found for Fe-Mn crusts (Wu et al., 2016).

Notably, as illustrated in Fig. 5c, the $\delta^{51}V_{AA}$ values of the larger tributary rivers (CW-2: Youshui River, CW-6: Wuyang River) and the two Yangtze River samples downstream of the Three-Gorges Dam can be grouped because of having the highest $\delta^{51}V_{AA}$ values (-0.45 ‰ to -0.13 ‰) and also the highest Fe load in the filters. These values are significantly higher than the values reported so far for granites of the continental crust. Weathering of rather exotic V-containing minerals (Schuth et al., 2017) may have the potential of producing such high V isotope signatures in water, but we do not know the abundance and isotope signature of those rare V-rich minerals investigated by Schuth et al. (2017) in the Yangtze River basin. Moreover, the V isotope signatures of more common minerals that may incorporate V like amphibole, spinel, or some micas (like roscoelite, $K(V,Al,Mg)_2AlSi_3O_{10}(OH)_2$; e.g., Nriagu,

892 1998) are still unknown. It remains yet to be investigated (i) if V mobilization by weathering
893 affects the V isotope composition of the dissolved V pool relative to its host rock signature,
894 and (ii) how efficient V adsorption fractionates the V isotope composition during riverine
895 transport.
896
897 *Yangtze River* - The dissolved V isotope composition of the Yangtze River becomes
898 increasingly enriched in the heavy ^{51}V over a distance of ca. 1,300 km with $\delta^{51}V_{AA}$ of -0.79 ‰
899 of the Three-Gorges-Dam lake to -0.48 ‰ near Wuhan, and finally to -0.13 ‰ in Nanjing (Fig.
900 5c). At the same time, the dissolved V concentration shows little variation with values of 1.6
901 to 1.7 µg/L of V. However, in contrast to the almost identical dissolved V concentration
902 between Wuhan and Nanjing, the amount of particulate V and Fe increases significantly
903 between these two sampling points by ~37 % for V and ~60 % for Fe (Fig. 5a,c).
904 Because so far no common geogenic V source with the observed high $\delta^{51}V$ values is
905 known for the study area, we can only speculate now that (i) human activity increased the
906 particulate V and Fe concentration in the Yangtze River, thereby potentially overprinting the
907 natural V isotope signature also of the dissolved V fraction, and/or (ii) an exchange of V
908 adsorbed to particulate matter like Fe^{III}(oxyhydr)oxides with dissolved V takes place during
909 transport. Vanadates are known to be efficiently adsorbed by Fe^{III}(oxyhydr)oxides, and at
910 reducing conditions and typical surface temperatures, V^{3+} can also easily substitute Fe^{3+} in
911 goethite (e.g., Gustafsson, 2019; Schwertmann and Pfab, 1994). Opposite to the increasingly
912 high $\delta^{51}V$ values of the Yangtze River water, the sample CW-10 from the Three-Gorges-Dam
913 lake is marked by a very low $\delta^{51}V_{AA}$ value of -0.79 ‰, and has also a lower load of particulate
914 Fe and V. This low $\delta^{51}V_{AA}$ may be attributed to either (or both) (i) a geogenic V isotope
915 signature, because the value overlaps those of basalts (Wu et al., 2016) and black shales
916 from the Niutitang Formation (Brüske et al., 2015), or (ii) to V that is released from
917 particulate Fe (oxyhydr)oxides when these enter water levels of the lake that are low in
918 oxygen and thus potentially start to disintegrate (the height of the dam is 185 m).
919 Alternatively, the lake water may be simply less polluted than the downstream Yangtze River
920 water, thereby having preserved or at least exhibiting a less modified geogenic V signature.
921 The two filters of the lower Yangtze River (FCW-11: Wuhan, FCW-13: Nanjing) however point
922 to a more complex situation. The particulate $\delta^{51}V_{AA}$ value of FCW-11 (Wuhan) is with -1.58
923 ‰ (±0.28, 2s.d.) lower than the one of particulate V with -1.08 ‰ (±0.24, 2s.d.) of FCW-13

sampled in Nanjing. This change of V isotope compositions is linked with a concomitant increase of particulate V in the Yangtze River from Wuhan to Nanjing at constant amounts of dissolved V. At a first glance, this seems to be contradictive to the theory that adsorbed V should be enriched in the light ^{50}V (Wu et al., 2015).

At a closer look however, it is evident that all samples taken from the three largest rivers in the area (Wuyang River, Youshui River, Yangtze River) are marked by higher $\delta^{51}V$ values of the dissolved V fraction than the average value for granites and andesites (Wu et al. 2016). The same is true for the V isotope composition of the particulate V load as seen for FCW-6 (Wuyang River, city center of Yuping) that has a $\delta^{51}V_{AA}$ value of -1.56 ‰ (±0.01, 2s.d.), which is comparable to the Yangtze River near Wuhan. As noted above, the $\delta^{51}V$ signatures of the larger tributaries can be influenced by a mixture of different anthropogenic sources with individual $\delta^{51}V$ values, e.g. (i) an influx of oil-contaminated water that can contain significant amounts of V, (ii) dissolved V delivered into the rivers as waste from the chemical or steel industry, or (iii), due to a higher input of particles with high affinity to bind V such as Fe oxides to increase the adsorption-driven V isotope fractionation that would result in even higher $\delta^{51}V$ values in the dissolved V pool.

5.2.2 Vanadium isotope signatures of seawater

The results of the North Atlantic NASS-6 seawater reference analyses show that our V separation protocol is capable of both handling large amounts of sample solution (1 L in this case) and providing reproducible data. The $\delta^{51}V_{AA}$ value of +0.30 ‰ (±0.14, 2s.d., n=3) of our NASS-6 solution is in excellent agreement with the average value of +0.32 ‰ (±0.13, 2s.d.) reported by Wu et al. (2019). It also highlights that different separation protocols and MC-ICP-MS machine parameters can produce similar results. Moreover, as demonstrated in comparison with our study, lower V yields of ca. 75 % as observed by Wu et al. (2019) show that such a loss is not incurring significant V fractionation. Our approach is especially helpful when larger amounts of sample solution (larger than the recommended maximum of 250 mL for the Nobias PA-1 resin) need to be processed in a timely fashion and without splitting the sample onto several columns in parallel. The latter approach may result in V loss (e.g. by poor adjustment of the pH in the first separation step) and/or a higher blank contribution. Furthermore, with respect to the UV-irradiated NASS-6 reference material, we were able to recover over 90 % of the loaded V until after the final purification step. Consequently, we

assume that both UV-irradiation and separating the V fraction at a pH=5 instead of pH=6 can contribute to this higher V recovery rate.

The North Sea water reveals an average $\delta^{51}V_{AA}$ value of +0.03 ‰ (±0.19, 2s.d., n=17) which is slightly lower than the average seawater $\delta^{51}V_{AA}$ value of +0.20 ‰ ±0.15 (2s.d.), and the results given for the North Atlantic, the Gulf of Mexico, and the North Pacific given by Wu et al. (2019). The North Sea water's V isotope signature is therefore framed by a slightly lower value represented by the lower Yangtze River (-0.13 ‰, sample CW-13, ~300 km upstream of the estuary) and the ocean water represented by e.g. the Gulf of Mexico (+0.22 ‰; Wu et al., 2019). However, the North Sea sample does not represent an open ocean water sample in a strict sense, but was taken in the Wadden area near the coast and the island of Spiekeroog, and ca. 40 km west of the estuary of the Weser River. Consequently, the water in the sampling area is most likely a mixture of river and seawater (see Beck et al., 2008, 2012; Kowalski et al., 2009). The slightly elevated V concentration of the North Sea sample of ~2 µg/L V relative to open ocean water (1.8 µg/L, Huang et al., 2015) can be attributed to (i) V-rich pore waters seeping out of the sediment at low tide, and/or (ii) desorption of V bound to particulate matter because of an increasing salinity from coast to open sea (Beck et al., 2008, 2012; Kowalski et al., 2009). According to Wu et al. (2015), desorption of V bound to particulate Fe oxides would result in a decrease of the $\delta^{51}V$ value of the dissolved V pool, because the adsorbed V is expected to be isotopically light. We do not know yet, however, the V isotope signatures of pore waters, hence an isotopic mass balance between V isotopic compositions of pore water, seawater, and river water is difficult to calculate for the North Sea. Nevertheless, the V isotope composition of the coastal North Sea water can also be explained as a mixture between continental run-off and open seawater signatures, as seen for the $\delta^{51}V_{AA}$ values of the lower Yangtze River and the average ocean water.

Conclusions

The method to separate V from seawater developed in this study offers an alternative approach to the procedure described by Wu et al. (2019), because it can handle larger volumes of seawater in a partly automated way and showed a V recovery of ≥90 % for the UV-irradiated NASS-6 seawater reference solution. Nevertheless, the results of this study

and the one of Wu et al. (2019) are in prefect agreement regarding the V isotope composition of NASS-6 with a proposed value of +0.30 ‰ ±0.14 (2s.d., this study) vs. +0.32 ‰ ±0.13 (Wu et al., 2019). First $\delta^{51}V_{AA}$ values of a water sample from the German North Sea coast scatter around +0.03 ‰ (±0.19 ‰, 2s.d.), and are slightly lower than the average open ocean value of +0.20 ‰ ±0.15 proposed by Wu et al. (2019). We attribute this slight offset to the sampling environment, i.e. an area strongly affected by the tides and the influx of brackish river water.

In this study we have reported the first $\delta^{51}V$ signatures of river water of the Yangtze River Basin, including the Yangtze River and some of its tributaries and sources. The source, smaller rivers, and the water of the Three-Gorges-Dam lake are marked by rather low $\delta^{51}V$ values scattering between -0.8 and -0.4 ‰ for the dissolved V fraction, and potentially reflect a host rock signature. In contrast to the tributaries, the high $\delta^{51}V$ signatures of dissolved V of -0.4 to -0.1 ‰ in the large rivers of the Yangtze River Basin may be the result of (i) preferential adsorption of ^{50}V onto particulate matter, in particular Fe (oxyhydr)oxides, as discussed by Wu et al. (2015), and/or (ii) at least partially generated by one or more anthropogenic sources.

The particulate V isotope signature is typically marked by comparatively lower $\delta^{51}V_{AA}$ values ranging from -2.2 ‰ to -0.1 ‰, but particulate V represents typically 30 % or even less of the total V budget in our sample suite. The average dissolved $\delta^{51}V$ value of all samples collected in the eastern Yangtze River Basin is -0.53 ‰ ±0.20 and therefore well matching the estimated value of -0.6 ‰ ±0.3 of Wu et al. (2019). When combining the V budgets and V isotope signatures of the dissolved and particulate V pools (eqn. 3), the average run-off of the Yangtze River Basin has a $\delta^{51}V_{AA}$ of -0.65 ‰ (±0.39, 2s.d.). The fine scale sampling and characterization of the V concentrations and V isotopic compositions conducted here for the Yangtze River system however clearly demonstrates that averaging the signatures for a "whole" river system may blur the complex V isotopic heterogeneity present along and within a river system, which may reveal the different factors influencing these V isotopic fractionation processes (anthropogenic, weathering, bioactivity, and adsorption).

The results of this work are a major step forward to understand the global V cycle and may be further exploited for V isotope variations of terrestrial and marine sediments of the early Earth. Still there are some parts of this cycle poorly constrained, e.g. V mobilization

respective fixation in sediments, and the V input into the ocean at mid-ocean ridge systems, thus requiring further investigation.

Acknowledgements

We wish to thank the Universities of Nanjing and Wuhan for their exceptional support during the sampling campaign. From University of Hannover, Alexandra Tangen is thanked for support in the clean laboratory, and Ingo Horn for keeping the mass spectrometers operational. Financial support by the DFG (German Research Foundation, grant SCHU-2695/5-1, and grant SCHU-2695/4 as part of the SPP-1833 project "Building a habitable Earth"), the NSFC (National Natural Science Foundation of China, grant no. 41650110480), the Fundamental Research Funds for the Central Universities (grant no. CUGCJ1709), and the special fund from the State Key Laboratory of Geological Processes and Mineral resources, China University of Geosciences (grant no. MSFGPMR03-2), is gratefully acknowledged. In addition, Sebastian Viehmann received funding for his field work in the P.R. China from the European Union's Horizon 2020 research and innovation program under the Marie Sklodowska-Curie project ELEMIN (grant no. 746033).

References

Abbasse, G., Ouddane, B., Fischer, J.C., 2002. Determination of trace levels of dissolved vanadium in seawater by use of synthetic complexing agents and inductively coupled plasma-atomic emission spectroscopy (ICP-AES). Anal. Bioanal. Chem. 374, 873–878. https://doi.org/10.1007/s00216-002-1532-3

Algeo, T.J., Kuwahara, K., Sano, H., Bates, S., Lyons, T., Elswick, E., Hinnov, L., Ellwood, B., Moser, J., Maynard, J.B., 2011. Spatial variation in sediment fluxes, redox conditions, and productivity in the Permian-Triassic Panthalassic Ocean. Palaeogeogr. Palaeoclimatol. Palaeoecol. 308, 65–83. https://doi.org/10.1016/j.palaeo.2010.07.007

Algeo, T.J., Maynard, J.B., 2004. Trace-element behavior and redox facies in core shales of Upper Pennsylvanian Kansas-type cyclothems. Chem. Geol. 206, 289-318.

Allison, J.D., Brown, D.S., Novo-Gradac, K.J., 1994. MINTEQA2/PRODEFA2. A geochemical assessment model for environmental systems. U.S. EPA, Athens, GA 30613, USA EPA/600/3-91/021.

Anbar, A.D., 2004. Iron stable isotopes: Beyond biosignatures. Earth Planet. Sci. Lett. 217, 223–236. https://doi.org/10.1016/S0012-821X(03)00572-7

Bauer, G., Günther, V., Hess, H., Otto, A., Roidl, O., Roller, H., Sattelberger, S., 2012. *Vanadium and vanadium compounds. Ullmann's Encyclopedia of Industrial Chemistry*. Wiley-VCH Verlag GmbH & Co., KGaA, Weinheim, Germany.

1057 Beck, M., Dellwig, O., Fischer, S., Schnetger, B., Brumsack, H.J., 2012. Trace metal
1058 geochemistry of organic carbon-rich watercourses draining the NW German coast.
1059 Estuar. Coast. Shelf Sci. 104–105, 66–79. https://doi.org/10.1016/j.ecss.2012.03.025
1060 Beck, M., Dellwig, O., Schnetger, B., Brumsack, H.J., 2008. Cycling of trace metals (Mn, Fe,
1061 Mo, U, V, Cr) in deep pore waters of intertidal flat sediments. Geochim. Cosmochim.
1062 Acta 72, 2822–2840. https://doi.org/10.1016/j.gca.2008.04.013
1063 Becker, J.S., Dietze, H.J., 1998. Inorganic trace analysis by mass spectrometry. Spectrochim.
1064 acta, Part B At. Spectrosc. 53, 1475–1506. https://doi.org/10.1016/S0584-
1065 8547(98)00110-4
1066 Berglund, M., Wieser, M.E., 2011. Isotopic compositions of the elements 2009 (IUPAC
1067 technical report). Pure Appl. Chem. 83, 397-410.
1068 Bjerrum, C.J., Canfield, D.E., 2004. New insights into the burial history of organic carbon on
1069 the early Earth. Geochemistry, Geophys. Geosystems 5, 1–9.
1070 https://doi.org/10.1029/2004GC000713
1071 Bredberg, K., Karlsson, H.T., Holst, O., 2004. Reduction of vanadium(V) with Acidithiobacillus
1072 ferrooxidans and Acidithiobacillus thiooxidans. Bioresour. Technol. 92, 93–96.
1073 https://doi.org/10.1016/j.biortech.2003.08.004
1074 Breit, G.N., Wanty, R.B., 1991. Vanadium accumulation in carbonaceous rocks: A review of
1075 geochemical controls during deposition and diagenesis. Chem. Geol. 91, 83–97.
1076 https://doi.org/10.1016/0009-2541(91)90083-4
1077 Brennecka, G.A., Herrmann, A.D., Algeo, T.J., Anbar, A.D., 2011. Rapid expansion of oceanic
1078 anoxia immediately before the end-Permian mass extinction. Proc. Natl. Acad. Sci. 108,
1079 17631–17634. https://doi.org/10.1073/pnas.1106039108
1080 Brinza, L., Benning, L.G., Statham, P.J., 2008. Adsorption studies of Mo and V onto
1081 ferrihydrite. Mineral. Mag. 72, 385–388.
1082 https://doi.org/10.1180/minmag.2008.072.1.385
1083 Brumsack, H.J., 2006. The trace metal content of recent organic carbon-rich sediments:
1084 Implications for Cretaceous black shale formation. Palaeogeogr. Palaeoclimatol.
1085 Palaeoecol. 232, 344–361. https://doi.org/10.1016/j.palaeo.2005.05.011
1086 Brüske, A., Schuth, S., Xu, L., Arnold, M.-C., Pierau, N., Weyer, S., 2015. Vanadium isotopes -
1087 a potential new proxy for paleo-oceanography. Goldschmidt Abstracts, 2015 411.
1088 Bruyère, V.I.E., García Rodenas, L.A., Morando, P.J., Blesa, M.A., 2001. Reduction of
1089 vanadium(V) by oxalic acid in aqueous acid solutions. J. Chem. Soc., Dalton Trans.,
1090 2001, 3593-3597.
1091 Catling, D.C., Claire, M.W., 2005. How earth's atmosphere evolved to an oxic state: A status
1092 report. Earth Planet. Sci. Lett. 237, 1–20. https://doi.org/10.1016/j.epsl.2005.06.013
1093 Chen, X., Wei, G., Deng, W., Liu, Y., Sun, Y., Zeng, T., Xie, L., 2015. Decadal variations in trace
1094 metal concentrations on a coral reef: Evidence from a 159 year record of Mn, Cu, and
1095 V in a *Porites* coral from the northern South China Sea. J. Geophys. Res. Oceans 120,
1096 405-416.
1097 Chester, R., 2000. *Marine Geochemistry*. Blackwell Science Ltd., Oxford, UK.
1098 Das, A., Krishnaswami, S., 2007. Elemental geochemistry of river sediments from the Deccan
1099 Traps, India: Implications to sources of elements and their mobility during basalt-water
1100 interaction. Chem. Geol. 242, 232–254.
1101 https://doi.org/10.1016/j.chemgeo.2007.03.023
1102 Emerson, S.R., Huested, S.S., 1991. Ocean anoxia and the concentrations of molybdenum
1103 and vanadium in seawater. Mar. Chem. 34, 177-196.
1104 Erbacher, J., Huber, B.T., Norris, R.D., Markey, M., 2001. Increased thermohaline

stratification as a possible cause for an ocean anoxic event in the cretaceous period. Nature 409, 325–327. https://doi.org/10.1038/35053041
German, C.R., Campbell, A.C., Edmond, J.M., 1991. Hydrothermal scavenging at the Mid-Atlantic Ridge: Modification of trace element dissolved fluxes. Earth Planet. Sci. Lett. 107, 101–114. https://doi.org/10.1016/0012-821X(91)90047-L
Gregory, D.D., Lyons, T.W., Large, R.R., Jiang, G., Stepanov, A.S., Diamond, C.W., Figueroa, M.C., Olin, P., 2017. Whole rock and discrete pyrite geochemistry as complimentary tracers of ancient ocean chemistry: An example from the Neoproterozoic Doushantuo Formation, China. Geochim. Cosmochim. Acta 216, 201-220.
Gustafsson, J.P., 2019. Vanadium geochemistry in the biogeosphere –speciation, solid-solution interactions, and ecotoxicity. Appl. Geochemistry 102, 1–25. https://doi.org/10.1016/j.apgeochem.2018.12.027
Gustafsson, J.P., Persson, I., Kleja, D.B., van Schaik, J.W.J., 2007. Binding of iron(III) to organic soils: EXAFS spectroscopy and chemical equilibrium modeling. Environ. Sci. Technol. 41, 1232-1237.
Huang, J.H., Huang, F., Evans, L., Glasauer, S., 2015. Vanadium: Global (bio)geochemistry. Chem. Geol. 417, 68–89. https://doi.org/10.1016/j.chemgeo.2015.09.019
Johnson, C.M., Beard, B.L., Roden, E.E., 2008. The Iron Isotope Fingerprints of Redox and Biogeochemical Cycling in Modern and Ancient Earth. Annu. Rev. Earth Planet. Sci. 36, 457–493. https://doi.org/10.1146/annurev.earth.36.031207.124139
Jeandel, C., Caisso, M., Minster, J.F., 1987. Vanadium behaviour in the global ocean and in the Mediterranean Sea. Mar. Chem. 21, 51-74.
Kendall, B., Brennecka, G.A., Weyer, S., Anbar, A.D., 2013. Uranium isotope fractionation suggests oxidative uranium mobilization at 2.50Ga. Chem. Geol. 362, 105–114. https://doi.org/10.1016/j.chemgeo.2013.08.010
Kowalski, N., Dellwig, O., Beck, M., Grunwald, M., Fischer, S., Piepho, M., Riedel, T., Freund, H., Brumsack, H.-J., Böttcher, M.E., 2009. Trace metal dynamics in the water column and pore waters in a temperate tidal system: response to the fate of algae-derived organic matter. Ocean Dynamics 59, 333-350.
Lapina, O.B., Bal'zhinimaev, B.S., Boghosian, S., Eriksen, K.M., Fehrmann, R., 1999. Progress on the mechanistic understanding of SO2 oxidation catalysts. Catal. Today 51, 469–479. https://doi.org/10.1016/S0920-5861(99)00034-6
Large, R.R., Halpin, J.A., Lounejeva, E., Danyushevsky, L.V., Maslennikov, V.V., Gregory, D., Sack, P.J., Haines, P.W., Long, J.A., Makoundi, C., 2015b. Cycles of nutrient trace elements in the Phanerozoic ocean: Gondwana Res. 28, 1282-1293.
Lau, K.V., Macdonald, F.A., Maher, K., Payne, J.L., 2017. Uranium isotope evidence for temporary ocean oxygenation in the aftermath of the Sturtian Snowball Earth. Earth Planet. Sci. Lett. 458, 282-292.
Lewan, M.D., Maynard, J.B., 1982. Factors controlling enrichment of vanadium and nickel in the bitumen of organic sedimentary rocks. Geochim. Cosmochim. Acta 46, 2547–2560. https://doi.org/10.1016/0016-7037(82)90377-5
Leya, I., Schönbächler, M., Wiechert, U., Krähenbühl, U., Halliday, A.N., 2007. High precision titanium isotope measurements on geological samples by high resolution MC-ICPMS. Int. J. Mass Spectrom. 262, 247–255. https://doi.org/10.1016/j.ijms.2006.12.001
Li, L., Kim, S., Wang, W., Vijayakumar, M., Nie, Z., Chen, B., Zhang, J., Xia, G., Hu, J., Graff, G., Liu, J., Yang, Z., 2011. A stable vanadium redox-flow battery with high energy density for large-energy density for large-scale energy storage. Adv. Energy Mater. 1, 394-400.

Lu, X.Q., Johnson, W.D., Hook, J., 1998. Reaction of vanadate with aquatic humic substances: An ESR and V-51 NMR study. Environ. Sci. Technol. 32, 2257-2263.
Lyons, T.W., Reinhard, C.T., Planavsky, N.J., 2014. The rise of oxygen in Earth's early ocean and atmosphere. Nature 506, 307–315. https://doi.org/10.1038/nature13068
Malinovsky, D., Kashulin, N.A., 2016. Vanadium isotope ratio measurements in fruit-bodies of: Amanita muscaria. Anal. Methods 8, 5921–5929. https://doi.org/10.1039/c6ay01436d
Montoya-Pino, C., Weyer, S., Anbar, A.D., Pross, J., Oschmann, W., van de Schootbrugge, B., Arz, H.W., 2010. Global enhancement of ocean anoxia during oceanic anoxic event 2: A quantitative approach using U isotopes. Geology 38, 315–318. https://doi.org/10.1130/G30652.1
Morford, J.L., Emerson, S., 1999. The geochemistry of redox sensitive trace metals in sediments. Geochim. Cosmochim. Acta 63, 1735–1750. https://doi.org/10.1016/S0016-7037(99)00126-X
Nielsen, S.G., Prytulak, J., Halliday, A.N., 2011. Determination of Precise and Accurate 51V/50V Isotope Ratios by MC-ICP-MS, Part 1: Chemical Separation of Vanadium and Mass Spectrometric Protocols. Geostand. Geoanalytical Res. 35, 293–306. https://doi.org/10.1111/j.1751-908X.2011.00106.x
Nielsen, S.G., Prytulak, J., Wood, B.J., Halliday, A.N., 2014. Vanadium isotopic difference between the silicate Earth and meteorites. Earth Planet. Sci. Lett. 389, 167–175. https://doi.org/10.1016/j.epsl.2013.12.030
Nriagu, J.O., 1998. *Vanadium in the environment*. John Wiley & Sons, New York, USA.
Parnell, J., Chen, H., Klubov, B., 2001. Hot oil in the Russian Arctic: Precipitation of vanadiferous bitumens, Novaya Zemlya. In *Mineral Deposits at the Beginning of the 21st Century* (eds. Piestrzyński, A., et al.). Swets & Zeitlinger B.V., Lisse, The Netherlands, pp. 71-74.
Prathap, K., Namasivayam, C., 2010. Adsorption of vanadate(V) on Fe(III)/Cr(III) hydroxide waste. Environ. Chem. Lett. 8, 363–371. https://doi.org/10.1007/s10311-009-0234-x
Prytulak, J., Nielsen, S.G., Halliday, A.N., 2011. Determination of Precise and Accurate 51V/50V Isotope Ratios by Multi-Collector ICP-MS, Part 2: Isotopic Composition of Six Reference Materials plus the Allende Chondrite and Verification Tests. Geostand. Geoanalytical Res. 35, 307–318. https://doi.org/10.1111/j.1751-908X.2011.00105.x
Prytulak, J., Nielsen, S.G., Ionov, D.A., Halliday, A.N., Harvey, J., Kelley, K.A., Niu, Y.L., Peate, D.W., Shimizu, K., Sims, K.W.W., 2013. The stable vanadium isotope composition of the mantle and mafic lavas. Earth Planet. Sci. Lett. 365, 177–189. https://doi.org/10.1016/j.epsl.2013.01.010
Prytulak, J., Sossi, P.A., Halliday, A.N., Plank, T., Savage, P.S., Woodhead, J.D., 2017. Stable vanadium isotopes as a redox proxy in magmatic systems? Geochemical Perspect. Lett. 75–84. https://doi.org/10.7185/geochemlet.1708
Rouxel, O.J., Bekker, A., Edwards, K.J., 2005. Archean and paleoproterozoic ocean redox state. Science 307, 1088-1091.
Saito, K., Tada, R., Zheng, H., Irino, T., Luo, C., He, M., Wang, K., Suzuki, Y., 2017. ESR signal intensity of quartz in the fine-silt fraction of riverbed sediments from the Yangtze River: a provenance tracer for suspended particulate matter. Prog. Earth Planet. Sci. 4, 4. https://doi.org/10.1186/s40645-017-0118-9
Schiffer, S., Liber, K., 2017a. Toxicity of aqueous vanadium to zooplankton and phytoplankton species of relevance to the Athabasca oil sands region. Ecotoxicol. Environ. Saf. 137, 1-11.

1201 Schiffer, S., Liber, K., 2017b. Estimation of vanadium water quality benchmarks for the
1202 protection of aquatic life with relevance to the Athabasca oil sands region using
1203 species sensitivity distributions. Environ. Toxicol. Chem. 36, 3034-3044.
1204 Schlesinger, W.H., Klein, E.M., Vengosh, A. 2017. Global biogeochemical cycle of vanadium.
1205 Proc. Natl. Acad. Sci., E11092-E11100.
1206 Schuth, S., Horn, I., Brüske, A., Wolff, P.E., Weyer, S., 2017. First vanadium isotope analyses
1207 of V-rich minerals by femtosecond laser ablation and solution-nebulization MC-ICP-MS.
1208 Ore Geol. Rev. 81. https://doi.org/10.1016/j.oregeorev.2016.09.028
1209 Schwertmann, U., Pfab, G., 1994. Structural vanadium in synthetic goethite. Geochim.
1210 Cosmochim. Acta 58, 4349–4352. https://doi.org/10.1016/0016-7037(94)90338-7
1211 Shen, Y., Buick, R., Canfield, D.E., 2001. Isotopic evidence for microbial sulphate reduction in
1212 the early Archean era. Nature 410, 77-81.
1213 Shiller, A.M., Boyle, E.A., 1987. Dissolved vanadium in rivers and estuaries. Earth Planet. Sci.
1214 Lett. 86, 214-224.
1215 Shiller, A.M., Mao, L., 2000. Dissolved vanadium in rivers: effects of silicate weathering.
1216 Chem. Geol. 165, 13-22.
1217 Shiller, A.M., Mao, L., 1999. Dissolved vanadium on the Louisiana Shelf: Effect of oxygen
1218 depletion. Cont. Shelf Res. 19, 1007–1020. https://doi.org/10.1016/S0278-
1219 4343(99)00005-9
1220 Shore, A., Fritsch, A., Heim, M., Schuh, A., Thoennessen, M., 2010. Discovery of the
1221 vanadium isotopes. At. Data Nucl. Data Tables 96, 351–357.
1222 https://doi.org/10.1016/j.adt.2010.02.002
1223 Smit, C.E., 2012. Environmental risk limits for vanadium in water. A proposal for water
1224 quality standards in accordance with the Water Framework Directive. RVIM Letter
1225 Report 601714021/2012. National Institute for Public Health and the Environment
1226 2012.
1227 Sohrin, Y., Bruland, K.W., 2011. Global status of trace elements in the ocean. TrAC - Trends
1228 Anal. Chem. 30, 1291–1307. https://doi.org/10.1016/j.trac.2011.03.006
1229 Sohrin, Y., Urushihara, S., Nakatsuka, S., Kono, T., Higo, E., Minami, T., Norisuye, K., Umetani,
1230 S., 2008. Multielemental determination of GEOTRACES key trace metals in seawater
1231 by ICPMS after preconcentration using an ethylenediaminetriacetic acid chelating
1232 resin. Anal. Chem. 80, 6767-6273.
1233 Soylak, M., Divrikli, U., Elci, L., Dogan, M., 2002. Preconcentration of Cr(III), Co(II), Cu(II),
1234 Fe(III) and Pb(II) as calmagite chelates on cellulose nitrate membrane filter prior to their
1235 flame atomic absorption spectrometric determinations. Talanta 56, 565–570.
1236 https://doi.org/10.1016/S0039-9140(01)00575-6
1237 Takeno, N., 2005. Atlas of Eh-pH diagrams Intercomparison of thermodynamic databases.
1238 Geol. Surv. Japan 47 i 270. https://doi.org/10.1063/1.3560359
1239 Templeton, G.D., Chasteen, N.D., 1980. Vanadium-fulvic acid chemistry: conformational and
1240 binding studies by electron spin probe techniques. Geochim. Cosmochim. Acta 44,
1241 741-752.
1242 Tribovillard, N., Algeo, T.J., Lyons, T., Riboulleau, A., 2006. Trace metals as paleoredox and
1243 paleoproductivity proxies: An update. Chem. Geol. 232, 12–32.
1244 https://doi.org/10.1016/j.chemgeo.2006.02.012
1245 Ueki, T., Adachi, T., Kawano, S., Aoshima, M., Yamaguchi, N., Kanamori, K., Michibata, H.,
1246 2003. Vanadium-binding proteins (vanabins) from a vanadium-rich ascidian Ascidia
1247 sydneiensis samea. Biochim. Biophys. Acta - Gene Struct. Expr. 1626, 43–50.
1248 https://doi.org/10.1016/S0167-4781(03)00036-8

Van Marwijk, J., Opperman, D.J., Piater, L.A., Van Heerden, E., 2009. Reduction of vanadium(V) by Enterobacter cloacae EV-SA01 isolated from a South African deep gold mine. Biotechnol. Lett. 31, 845–849. https://doi.org/10.1007/s10529-009-9946-z

Ventura, G.T., Gall, L., Siebert, C., Prytulak, J., Szatmari, P., Hürlimann, M., Halliday, A.N., 2015. The stable isotope composition of vanadium, nickel, and molybdenum in crude oils. Appl. Geochemistry 59, 104–117. https://doi.org/10.1016/j.apgeochem.2015.04.009

Wang, D., Sañudo-Wilhelmy, S.A., 2008. Development of an analytical protocol for the determination of V (IV) and V (V) in seawater: Application to coastal environments. Mar. Chem. 112, 72–80. https://doi.org/10.1016/j.marchem.2008.05.011

Wang, D., Sañudo Wilhelmy, S.A., 2009. Vanadium speciation and cycling in coastal waters. Mar. Chem. 117, 52–58. https://doi.org/10.1016/j.marchem.2009.06.001

Wang, Y., Yang, Z., Shen, Z., Tang, Z., Niu, J., Gao, F., 2011. Assessment of heavy metals in sediments from a typical catchment of the Yangtze River, China. Environ. Monit. Assess. 172, 407–417. https://doi.org/10.1007/s10661-010-1343-5

Wanty, R.B., Goldhaber, M.B., 1992. Thermodynamics and kinetics of reactions involving vanadium in natural systems: Accumulation of vanadium in sedimentary rocks. Geochim. Cosmochim. Acta 56, 1471-1483.

Wehrli, B., Stumm, W., 1989. Vanadyl in natural waters: Adsorption and hydrolysis promote oxygenation. Geochim. Cosmochim. Acta 53, 69–77. https://doi.org/10.1016/0016-7037(89)90273-1

Weyer, S., Schwieters, J.B., 2003. High precision Fe isotope measurements with high mass resolution MC-ICPMS. Int. J. Mass Spectrom. 226, 355–368. https://doi.org/10.1016/S1387-3806(03)00078-2

Wright, M.T., Stollenwerk, K.G., Belitz, K., 2014. Assessing the solubility controls on vanadium in groundwater, northeastern San Joaquin Valley, CA. Appl. Geochemistry 48, 41–52. https://doi.org/10.1016/j.apgeochem.2014.06.025

Wu, F., Qi, Y., Yu, H., Tian, S., Hou, Z., Huang, F., 2016. Vanadium isotope measurement by MC-ICP-MS. Chem. Geol. 421, 17–25. https://doi.org/10.1016/j.chemgeo.2015.11.027

Wu, F., Qin, T., Li, X., Liu, Y., Huang, J.H., Wu, Z., Huang, F., 2015. First-principles investigation of vanadium isotope fractionation in solution and during adsorption. Earth Planet. Sci. Lett. 426, 216–224. https://doi.org/10.1016/j.epsl.2015.06.048

Xu, L., Lehmann, B., Mao, J., 2013. Seawater contribution to polymetallic Ni-Mo-PGE-Au mineralization in Early Cambrian black shales of South China: Evidence from Mo isotope, PGE, trace element, and REE geochemistry. Ore Geol. Rev. 52, 66–84. https://doi.org/10.1016/j.oregeorev.2012.06.003

Xu, L., Lehmann, B., Mao, J., Nägler, T.F., Neubert, N., Böttcher, M.E., Escher, P., 2012. Mo isotope and trace element patterns of Lower Cambrian black shales in South China: Multi-proxy constraints on the paleoenvironment. Chem. Geol. 318–319, 45–59. https://doi.org/10.1016/j.chemgeo.2012.05.016

Zhang, J., Dong, H., Zhao, L., McCarrick, R., Agrawal, A., 2014. Microbial reduction and precipitation of vanadium by mesophilic and thermophilic methanogens. Chem. Geol. 370, 29–39. https://doi.org/10.1016/j.chemgeo.2014.01.014

Zhou, X., Wei, C., Li, M., Qiu, S., Li, X., 2011. Thermodynamics of vanadium-sulfur-water systems at 298 K. Hydrometallurgy 106, 104–112. https://doi.org/10.1016/j.hydromet.2010.12.003

1297

1298 Electronic Appendix

1299

1300 Method details

1301

1302 A1 Chemicals

1303 All employed acids in this study were purified by sub-boiling distillation in either a
1304 conventional infra-red heated quartz glass still (for HNO_3) or a Teflon cupola still (for HCl;
1305 PicoTrace, Germany) from commercially available *pro analysis* grade acids.

1306 Purified water (18.2 MΩ grade) was produced by a Millipore Milli-Q system
1307 (Karlsruhe, Germany).

1308 The cation resin (Bio-Rad® AG 50WX12, 200-400 mesh) and the anion resin (Bio-Rad®
1309 AG 1X8, 200-400 mesh) were cleaned before use stepwise twice with purified water, 2 M
1310 HCl, water, 5 M HCl, and 2 M HCl, respectively. These resins were stored in 2 M HCl.

1311 The Bio-Rad® Chelex-100 resin (1 % cross-linkage, 100-200 mesh, Na^+ form) uses
1312 styrene divinylbenzene copolymers as a carrier. Prior to loading into the PP columns, it was
1313 cleaned and conditioned as shown in Table S1 (Electronic Appendix).

1314 All other chemicals, 30 % H_2O_2, 25 % NH_3, 100 % acetic acid, employed in this study
1315 were of *suprapure* grade and purchased from commercial providers.

1316

1317 A2 Columns

1318 Ready-made PP (poly-propylene, Bio-Rad® Laboratories Inc., USA) columns with a
1319 total volume of 10 mL (including a 2mL resin reservoir) were employed to separate V from
1320 major elements (e.g., Ca, Na, K,) and trace elements (Ti, Fe, Cr) by either filling them with
1321 cation resin or anion resin (Table 2). A final purification step (step 3) required micro-columns
1322 that were prepared from conventional 1 mL pipette tips and a frit made of HDPE (high-
1323 density polyethylene, pore size 35 µm; purchased from RCT GmbH & Co., Germany).

1324 The Chelex-100 resin for initial V separation from the seawater matrix was loaded
1325 into pre-cleaned PP columns (Rockbourne Scientific, UK) with a length of 15 cm, a diameter
1326 of 1 cm, and total volume 20 mL. This resulted in a resin height of ca. 5-6 cm. The resin was
1327 washed with two column volumes (cv) of 1 M ammonium-acetate buffer solution prior to
1328 sample loading.

All columns were cleaned step-wise with purified water, diluted alkaline detergent (Elma Clean, Germany), water, and ~5 % HCl over several days prior to loading with resin.

A3 Bottles and filtration device

All samples were stored in LDPE (low-density polyethylene, 3 L volume) bottles for transport. Prior to use, these bottles were rinsed with de-ionized water and then filled with ca. 1 M HNO_3 to remove potential contaminants for several days.

The employed filters (47 mm diameter, 0.45 µm pore size; Sartorius-Stedim, Germany) are made of cellulose nitrate, and fit into the polycarbonate filtration device type 16510 of Sartorius GmbH (Germany) that was connected to a small pump (KNF Labs, France). After use, they were placed onto and carefully covered by clean laboratory paper tissue for air-drying overnight. After drying, the filters were stored in small LDPE laboratory bags for transport in a box preventing bending or breaking of the dry filter material. After each sample filtration, the filter device was disassembled, rinsed with tap water, wiped with laboratory tissue, rinsed again with 3 % HNO_3, and finally rinsed with purified water before drying. For transport, the parts of the device were stored in clean and sealed laboratory plastic bags.

A4 Microwave Digestion

The filters were dissolved overnight in concentrated HNO_3 at 85 °C on a hot plate (see also Soylak et al., 2012). After drying of the solution, a digestion step using 6 mL aqua regia at 130 °C followed to further break down organic compounds. After drying, chlorine was removed by covering the samples with 5 mL 1 M HNO_3, followed by another drying step. To eliminate any remaining organic matter, the residues were dissolved again in 20 mL concentrated HNO_3, and transferred into 100 mL Teflon vials for microwave-induced digestion. After being firmly closed, they were placed in a MLS Start 640 microwave system (MLS, Germany), and digested for 45 minutes at 180 °C after a heating ramp of 45 minutes. When the solutions had cooled, they were transferred again into Teflon beakers, dried, and taken up in 5 mL of 3 M HNO_3. After centrifugation at 4,000 rpm for 10 minutes, gravimetric dilutions of 1:500 were prepared from aliquots for ICP-MS analyses as described above. The remaining solution was dried in preparation of the V separation protocol.

A5 SF-ICP-MS analyses

Aliquots of the river water and the digested filter samples were aspired through a PFA (perfluoroalkoxy alkane; Elemental Scientific, Germany) nebulizer with an uptake rate of ~100 µL/min into a double-pass quartz glass spray chamber (Scott design, Thermo Scientific, Germany). Conventional sampler and skimmer cones (H type, Ni) were used during ICP-MS analyses employing a Thermo-Scientific Element XR fast scanning-high resolution-sector field-ICP-MS. For the seawater samples, a jet-type sampler and a H-type skimmer cone, a cyclonic quartz glass spray chamber (Glass Expansion, Australia) and a glass nebulizer (Meinhard, USA) were installed instead to cope with the high salt load and low trace metal levels of these samples. Solutions with element concentrations (including Ti, V, Cr, Fe, and others) of 0.1, 1, 10, and 100 µg/L were prepared from MIX-1 and MIX-2 multi-element solutions available from LGC Standards (Germany) to yield a calibration line.

Figure

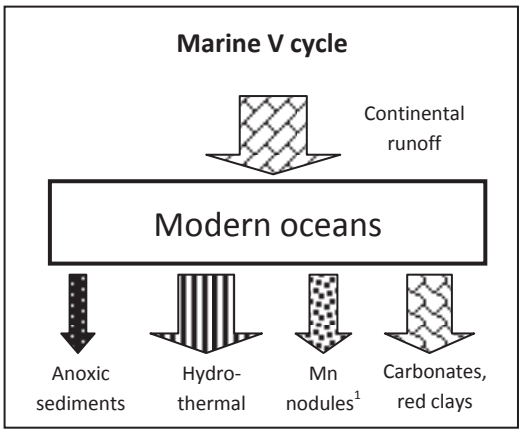

Fig. 1. A simplified overview of vanadium sources and sinks in the marine environment. (1) Is representative of metalliferous sediments and Fe-Mn nodules. After Morford & Emerson (1999).

Figure

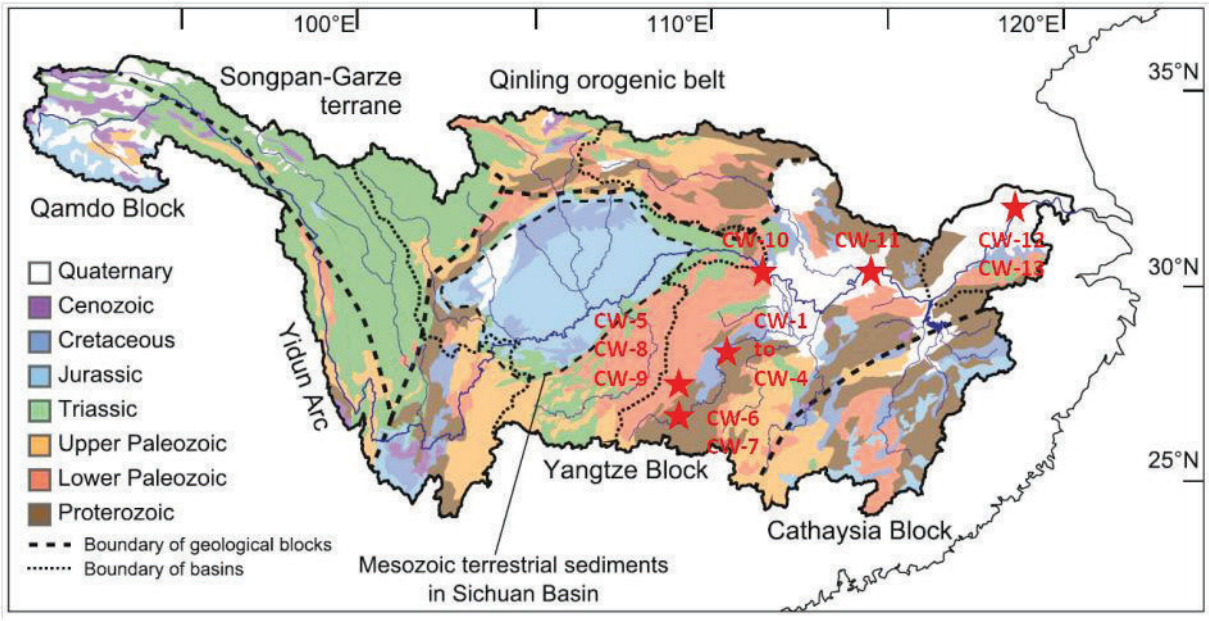

Fig. 2. Geology and major rivers of the Yangtze River Basin. The sample areas are marked by red stars (see also Table 1 for detailed sample locations). Slightly modified from Saito et al. (2017).

Figure

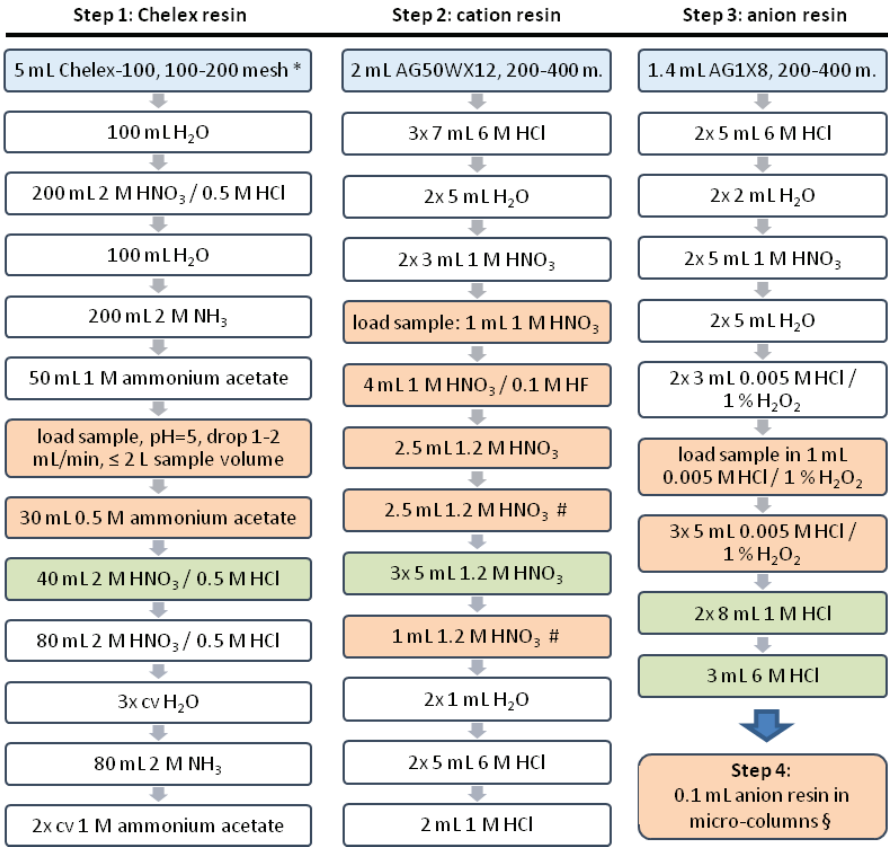

Fig. 3. Illustration of the V purification procedure for seawater and river samples developed in this study. Step 1 (Chelex resin) was adopted from Abbasse et al. (2002), step 2 (cation resin) was slightly modified after Wu et al. (2016), and step 3 (anion resin) was adopted from Schuth et al. (2017). Brown fields highlight matrix elution, green fields the V fraction. Between each column step, the V fraction was treated with aqua regia to remove potential organic contribution of the resin.

(*) The Chelex-100 resin was conditioned to the NH_4^+ form before loading.

(#) These cuts were checked by ICP-MS for V to avoid a potential V loss.

(§) Step 4 shown in the lower right corner of the sketch employs micro-columns (see text), but otherwise follows step 3 with all solution volumes reduced by factor 10 (see also Wu et al., 2016).

(cv) Column volume.

Figure

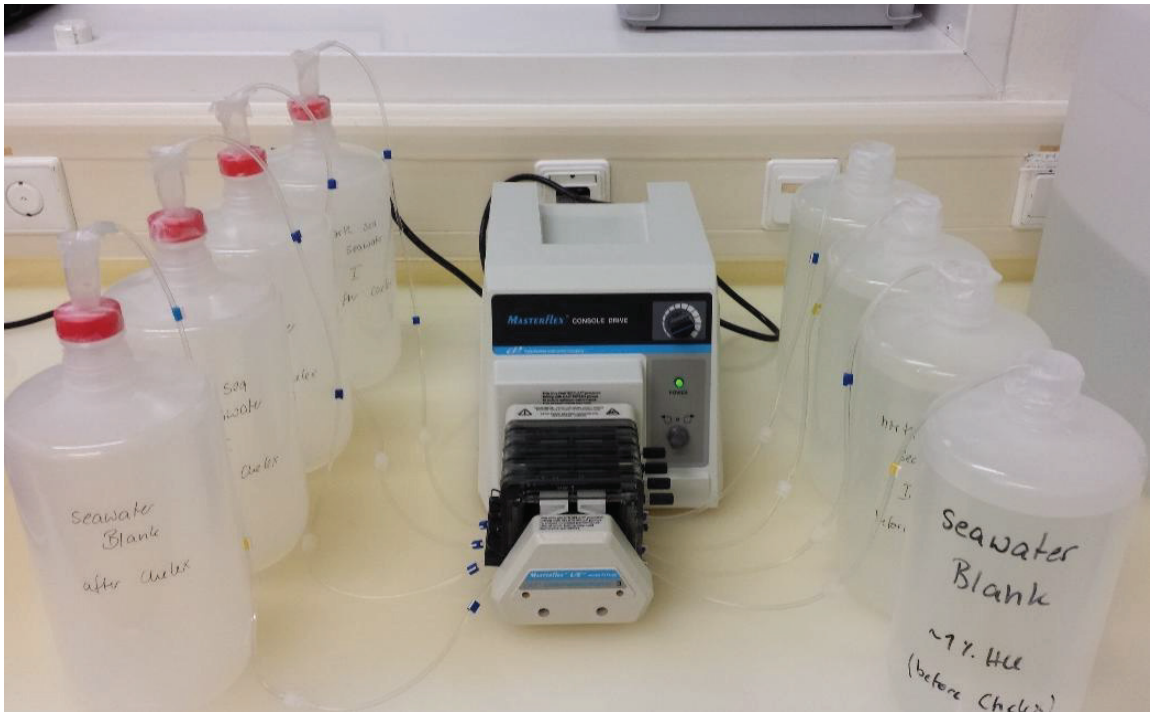

Fig. 3. Loading seawater samples (right side) onto the Chelex-100 resin in PP columns mounted on LDPE bottles to collect the matrix (left side). A 4-channel peristaltic pump (center) transfers the sample solutions at a rate of 1-2 mL/min through Tygon tubes.

Figure

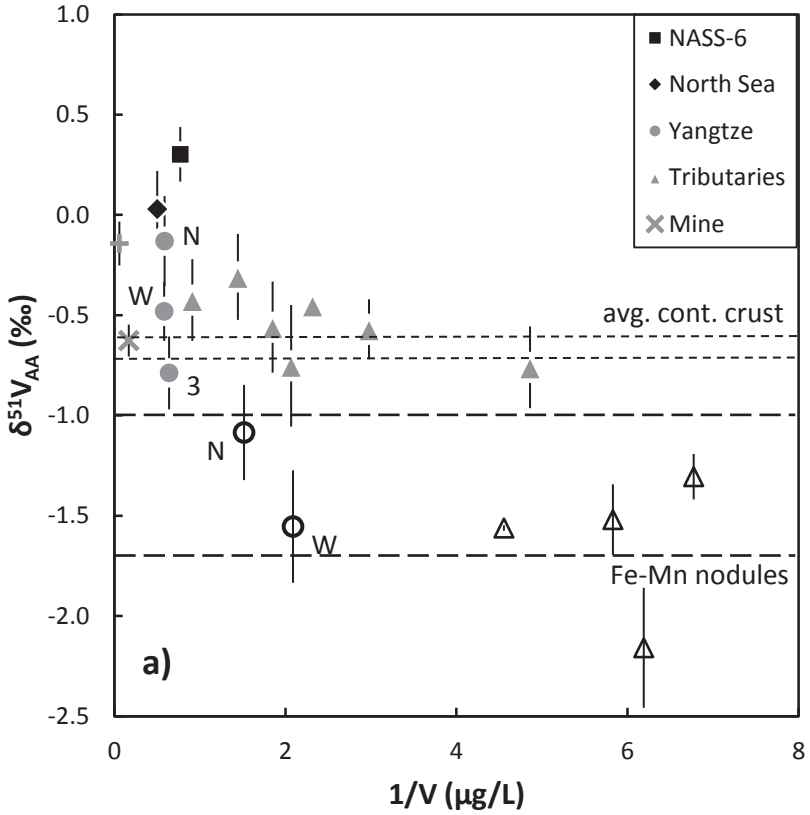
NASS-6
North Sea
Yangtze
Tributaries
Mine
avg. cont. crust
Fe-Mn nodules
N
W
3
N
W
a)
$\delta^{51}V_{AA}$ (‰)
1/V (µg/L)

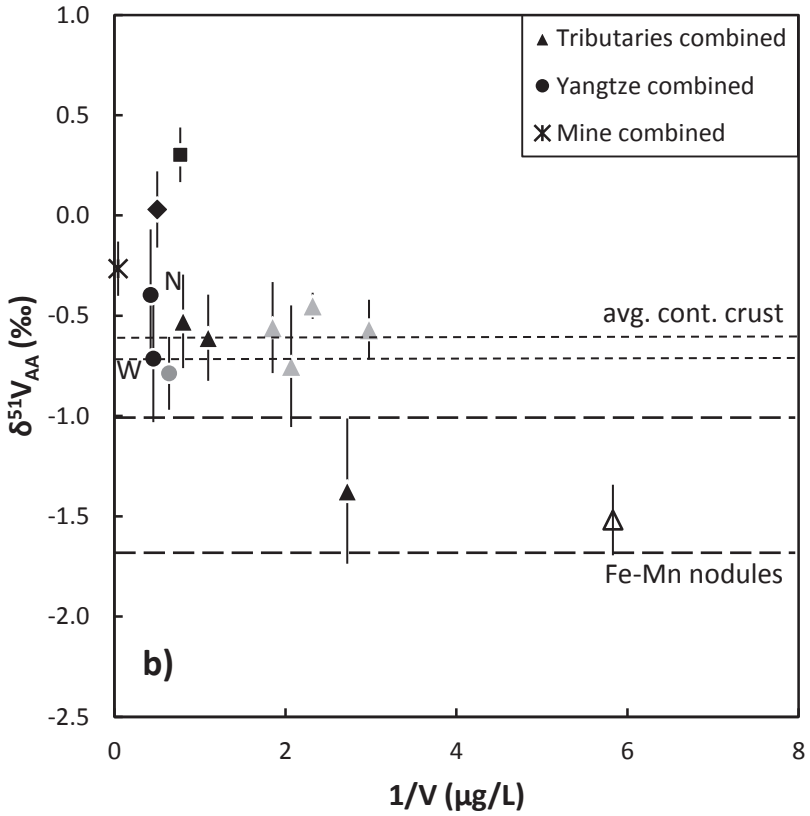
Tributaries combined
Yangtze combined
Mine combined
avg. cont. crust
Fe-Mn nodules
N
W
b)
$\delta^{51}V_{AA}$ (‰)
1/V (µg/L)

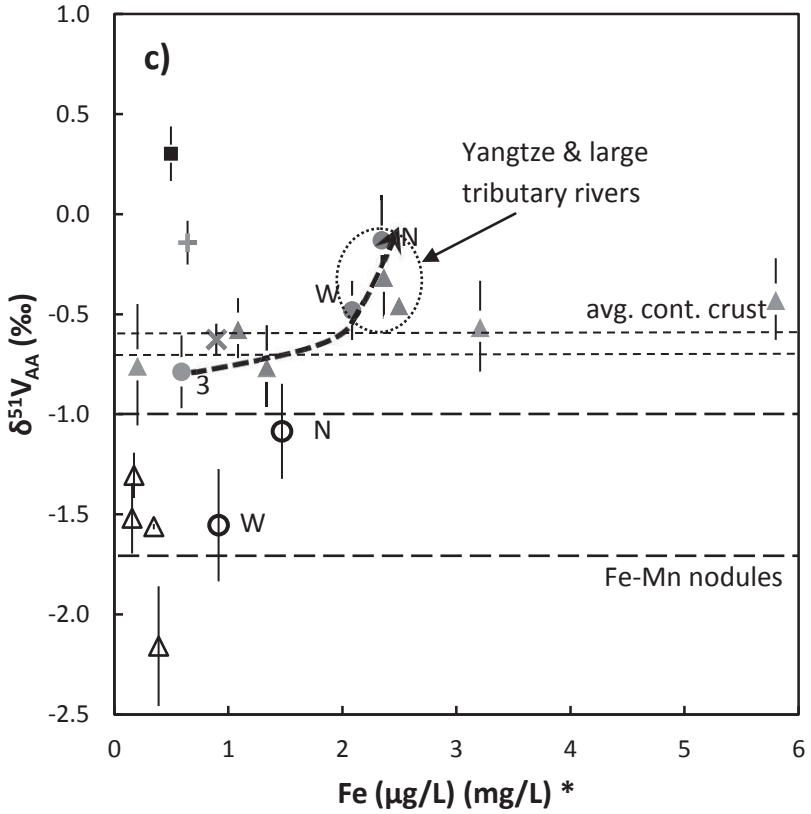

Fig. 5. Vanadium isotope systematics of this study. Closed grey symbols represent dissolved V concentrations and isotope compositions, open symbols represent results of particulate V. "W" and "N" denote the samples taken from the Yangtze River near the cities of Wuhan (CW-11) and Nanjing (CW-13), respectively, whereas "3" represents the sample of the Three-Gorges-Dam lake (CW-10). Seawater samples are shown by black filled symbols. The field of the average continental crust (thin stippled line) refers to average $\delta^{51}V$ values of an andesite (AGV-2) and quartz latite (QLO-1), and the field of Fe-Mn crusts (thick stippled line) to $\delta^{51}V$ values of the Fe-Mn nodules NOD-A and NOD-P (see Wu et al., 2016). Error bars are 2 standard deviation (2s.d.).

In (a), all results of this study are shown. For a better visualization, the V concentrations are given as 1/V.

In (b), V isotope compositions of dissolved and particulate V of some samples have been calculated to $\delta^{51}V_{Total}$ (marked as "combined") according to equation 3 (see text). They are shown by filled black symbols.

In (c), $\delta^{51}V$ values vs. Fe concentrations are shown. Particulate Fe concentrations and dissolved Fe of mine water (CW-3, marked by "x") have been divided by 1,000 for a better visualization, their concentrations are otherwise in mg/L (*). The black stippled arrow highlights $\delta^{51}V$-Fe variations of the Yangtze River samples towards higher $\delta^{51}V$ values of dissolved V at increasing Fe concentrations (both dissolved and particulate Fe).

Table

Click here to download Table: Schuth etal_Table-1.pdf

Table 1. Sample locations and sample volumes investigated in this study.

Sample	Water body	Location °N	Location °E	Next town/city	Volume (L)	# of filters	Volume for analyses (L) [1]	Comments
CW-1	Unnamed creek	29° 1.855'	110° 13.868'	Qingpingzhen	2.5	6	1.4	Small, shallow dam lake fed by a small creek emerging near an abandoned Ni-Mo mine in the Niutitang Formation.
CW-2	Youshui River	28° 44.291'	109° 56.474'	Furongzhen	2.4	3	1.7	Large river.
CW-3	Mine drainage	28° 30.113'	109° 56.621'	Xiangxi (29 km NE)	3.0	1	0.5	Effluent of an abandoned small underground U mine.
CW-4	Unnamed creek	28° 29.747'	109° 49.126'	Xiquetou (3 km N)	2.6	1	0.7	Small fast-flowing creek draining into the Longbi River. Water from CW-3 drains into the same creek.
CW-5	Pingtu River	28° 2.478'	109° 4.845'		3.3	3	3.3	Small fast-flowing river.
CW-6	Wuyang River	27° 14.164'	108° 54.211'	Yuping	3.2	2	1.1	Sample taken in the city center.
CW-7	Stream source	27° 10.050'	108° 52.778'		3.4	4	-	Water emerges between phosphorite and barite layers of the Niutitang Formation.
CW-8	Panxihe+Taiping Rivers	27° 49.901'	108° 45.678'	Panxi	3.4	1	2.2	Fast-flowing water collected at the confluence of the Panxihe and Taiping rivers.
CW-9	Unnamed creek	28° 1.732'	109° 6.257'		3.4	1	1.5	Small creek that enters the Pingtu River. Sample location ca. 2.7 km E of sample CW-5.
CW-10	Yangtze River	30° 49.906'	110° 58.808'	Zigui	3.4	4	0.5	Three-Gorges-Dam lake, sample location ca. 2.4 km W of the dam. Sample location is upstream of the large Lishui, Wu, and Yuan rivers. Heavy rainfall during sampling.
CW-11	Yangtze River	30° 23.014'	114° 9.727'	Wuhan	3.4	6	0.5	Industrial area SW of Wuhan. Sample location is downstream of the confluence of the large Lishui, Wu, and Yuan rivers, and drainage of Lake Dongting.
CW-12	Hot spring	32° 9.217'	118° 41.393'	Nanjing	3.5	1	-	Hot spring within the city. Handwarm water is used for washing and baths.
CW-13	Yangtze River	32° 7.771'	118° 46.929'	Nanjing	3.4	6	0.5	Sample taken within Nanjing.
North Sea	North Sea (German coast)	53° 45.016'	7° 40.266'	Spiekeroog	19	Not available	4	Sample collected and filtered at University Oldenburg.

(1) Volumes of river water dried for V isotope analyses.

Table

Click here to download Table: Schuth etal_Table-2.pdf

Table 2. Vanadium isotope compositions, and concentrations of V, Ti, Cr, and Fe in the river water samples (CW-x), filters (FCW-x), North Sea water, and reference material NASS-6 (North Atlantic). The analytical uncertainty is given as relative standard deviation (RSD, %). The concentrations in the filters have been recalculated to the solution volume of their respective samples. Note the high Fe concentrations in the filters.

Sample	V (µg/L)	*RSD (%)*	Ti (µg/L)	*RSD (%)*	Cr (µg/L)	*RSD (%)*	Fe (µg/L)[+]	*RSD (%)*	$\delta^{51}V_{AA}$ ‰	$\delta^{51}V_{NIST}$ ‰	*2s.d.*	n [#]	Remarks
CW-1	0.54	*1.9*	0.023*	*b.q.l.*	3.23	*1.0*	3.21	*8.4*	-0.56	-1.17	*0.23*	3	
FCW-1	*0.075*	*4.6*	*0.467*	*4.1*	*0.063*	*8.9*	*53,000*	*5.0*	-	-	-	-	V too low
CW-2	0.43	*7.1*	b.d.l.	-	3.20	*5.0*	2.50	*8.1*	-0.45	-1.06	*0.07*	3	
FCW-2	*0.105*	*5.4*	*0.284*	*3.9*	*0.096*	*2.9*	*61,000*	*4.1*	-	-	-	-	V too low
CW-3	5.97	*6.0*	b.d.l.	-	7.11	*6.4*	894,000	*6.3*	-0.63	-1.24	*0.08*	3	
FCW-3	*17.5*	*1.9*	*0.019*	*22*	*0.231*	*1.8*	*270,000*	*1.4*	-0.14	-0.75	*0.11*	3	
CW-4	1.10	*4.5*	b.d.l.	-	2.81	*5.2*	5.80	*3.7*	-0.42	-1.03	*0.20*	3	
FCW-4	*0.148*	*2.9*	*0.380*	*2.3*	*0.080*	*2.8*	*72,000*	*2.8*	-1.30	-1.91	*0.11*[§]	1	
CW-5	0.206	*6.1*	0.019*	*b.q.l.*	2.51	*1.3*	13.4	*3.1*	-0.76	-1.37	*0.20*	3	
FCW-5	*0.162*	*2.1*	*0.543*	*3.3*	*0.164*	*5.3*	*163,000*	*2.6*	-2.16	-2.77	*0.30*	2	
CW-6	0.693	*11*	b.d.l.	-	2.50	*11*	2.36	*11*	-0.31	-0.92	*0.21*	3	
FCW-6	*0.220*	*9.3*	*0.584*	*10*	*0.265*	*9.9*	*145,000*	*9.1*	-1.56	-2.17	*0.01*	2	
CW-7	0.067	*9.4*	0.067*	*b.q.l.*	2.34	*6.5*	40.1	*6.8*	-	-	-	-	V too low
FCW-7	*0.172*	*3.6*	*0.252*	*6.0*	*0.071*	*6.8*	*65,000*	*5.0*	-1.52	-2.13	*0.18*	2	
CW-8	0.336	*7.2*	b.d.l.	-	2.53	*3.9*	1.08	*7.3*	-0.57	-1.18	*0.15*	3	
FCW-8	*0.027*	*6.1*	*0.310*	*3.2*	*0.054*	*12*	*35,000*	*4.3*	-	-	-	-	V too low
CW-9	0.484	*3.5*	b.d.l.	-	2.52	*0.6*	0.202*	*b.q.l.*	-0.75	-1.36	*0.30*	3	
FCW-9	*0.068*	*6.9*	*0.364*	*8.0*	*0.048*	*6.7*	*34,000*	*4.8*	-	-	-	-	V too low
CW-10	1.57	*2.3*	0.018*	*b.q.l.*	2.55	*3.7*	0.588	*8.8*	-0.79	-1.40	*0.18*	3	
FCW-10	*0.060*	*1.7*	*1.44*	*2.4*	*0.078*	*2.6*	*40,000*	*1.0*	-	-	-	-	V too low
CW-11	1.72	*4.1*	0.004*	*b.q.l.*	2.51	*5.3*	2.08	*10*	-0.48	-1.09	*0.15*	3	
FCW-11	*0.479*	*0.9*	*5.57*	*1.6*	*0.563*	*2.8*	*385,000*	*1.6*	-1.55	-2.16	*0.28*	3	
CW-12	b.d.l.	-	b.d.l.	-	b.d.l.	-	144	*4.9*	-	-	-	-	V too low
FCW-12	*0.0003**	*b.q.l.*	*0.136*	*13*	*0.006*	*10*	*2,599*	*15*	-	-	-	-	V too low
CW-13	1.71	*5.6*	0.019*	*b.q.l.*	2.11	*5.7*	2.34	*3.5*	-0.13	-0.74	*0.22*	3	
FCW13	*0.660*	*0.5*	*3.77*	*1.4*	*0.815*	*2.0*	*619,000*	*1.6*	-1.08	-1.69	*0.24*	3	
North Sea IV	2.00	*15?*	1.89	*15?*	b.d.l.	-	b.d.l.	-	-0.06	-0.67	*0.19*	3	2 L sample split
North Sea V	2.00	*15?*	1.89	*15?*	b.d.l.	-	b.d.l.	-	+0.04	-0.57	*0.02*	2	2 L sample split
North Sea VI	2.00	*15?*	1.89	*15?*	b.d.l.	-	b.d.l.	-	+0.10	-0.50	*0.02*	2	2 L sample split
North Sea VIII	2.00	*15?*	1.89	*15?*	b.d.l.	-	b.d.l.	-	-0.12	-0.73	*0.22*	4	2 L sample split
North Sea IX	2.00	*15?*	1.89	*15?*	b.d.l.	-	b.d.l.	-	-0.09	-0.70	*0.20*	3	2 L sample split
North Sea +AA	5	*n.d.*	n.a.	-	n.a.	-	n.a.	-	-0.19	-	*0.23*	15	Doped with AA to 5 µg/L V
North Sea +NIST	5	*n.d.*	n.a.	-	n.a.	-	n.a.	-	-	-0.11	*0.19*	11	Doped with NIST to 5 µg/L V
NASS-6 (cert)	1.46	*12*	n.d.	-	0.118	*6.8*	0.495	*9.3*	+0.30	-0.31	*0.14*	3	UV irradiated

(+) The Fe concentrations of the filters have been rounded off the last three digits. (*) Below quantification limit, b.q.l. (b.d.l.) Below detection limit. (cert) Certified values of the NASS-6 reference material. (#) Number of analyses. (§) The reproducibility of the standards measured before and after this sample was used for calculation of the 2s.d. (n.d.) Not determined. (n.a.) Not analyzed.

Table

Click here to download Table: Schuth etal_Table-S1.pdf

Table S1: Pre-cleaning and conversion procedure of new Bio-Rad Chelex-100 resin.

Resin	Mobile phase	Volume	Comment
5 mL Chelex-100	H_2O	5 cv	Cleaning
100-200 mesh	1M HCl	2 cv	Cleaning, convert to H^+ form
(Na^+ form)	H_2O	5 cv	Cleaning
	2M NH_3	2 cv	Convert to NH_4^+ form
	H_2O	5 cv	Cleaning
	1M $NH_4CH_3CO_2$ (pH=5)	-	Storage in buffer solution

cv) column volume.

Table

Click here to download Table: Schuth etal_Table-S2.pdf

Table S2. Operating parameters of the MC-ICP-MS at University Hannover.

Mass spectrometer	Thermo-Scientific Neptune *Plus*/Neptune
RF power	1020 W / 1250 W
Reflected power	<2 W
Accelerating voltage	-9950 V
Resolution mode	High resolution
Cone material, types	Ni or Al, x-type skimmer cones
Carrier gas	Argon
Cool gas flow	13.5 L min^{-1}
Auxiliary gas flow	0.8 - 1.0 L min^{-1}
Nebulizer gas flow	~1.0 L min^{-1}
Nebulizer, uptake rate	CETAC[a] PFA[b], ~50 µL min^{-1}
Desolvator	CETAC Aridus II
Spray chamber temperature	110 °C
Membrane temperature	160 °C
Mass bias correction	Fe solution (IRMM-014) Exponential Law

Faraday detector setup

Neptune *Plus*

Detector	L5*	L4	L2	L1	H1	H2	H4
Mass	^{49}Ti	^{50}V	^{51}V	^{52}Cr	^{54}Fe	^{56}Fe	^{57}Fe
Resistor (Ω)	10^{11}	10^{11}	10^{10}	10^{11}	10^{11}	10^{11}	10^{11}

Neptune

Detector	L3	L2	L1	C	H1	H2	H4
Mass	^{49}Ti	^{50}V	^{51}V	^{52}Cr	^{53}Cr	^{54}Fe	^{56}Fe
Resistor (Ω)	10^{11}	10^{11}	10^{10}	10^{11}	10^{11}	10^{11}	10^{11}

(a) CETAC Technologies, USA. (b) Perfluoroalkoxy alkane. (*) The L5 detector is immovable, therefore all other detectors were aligned relative to the L5 detector.